

Meson and Isobar Degrees of Freedom in $A(\vec{e}, e'\vec{p})$ reactions at $0.2 \leq Q^2 \leq 0.8$ (GeV/c)²

Jan Ryckebusch *, Dimitri Debruyne, Wim Van Nespen and Stijn Janssen

Department of Subatomic and Radiation Physics

University of Gent, Proeftuinstraat 86, B-9000 Gent, Belgium

(February 6, 2020)

The effect of meson and isobar degrees of freedom in $A(\vec{e}, e'\vec{p})$ and $A(e, e'n)$ is studied for four-momentum transfers Q^2 in the range between 0.2 and 0.8 (GeV/c)². The calculations are performed in a non-relativistic framework with explicit (N, Δ, π) degrees-of-freedom. For the whole range of momentum transfers under investigation the relative effect of the meson-exchange and isobar degrees of freedom is significant. At low missing momenta and quasi-elastic conditions, a tendency to reduce the $(e, e'p)$ and $(e, e'n)$ differential cross sections is noticed. The greatest sensitivity is found in the interference structure functions W_{LT} and W_{TT} . The recoil polarization observables, on the other hand, are moderately affected by the meson-exchange and Δ -isobar currents.

I. INTRODUCTION

Systematic investigations of $A(e, e'p)$ reactions at Saclay, NIKHEF, Mainz and Bates have produced an impressive amount of data for various target nuclei [1]. For the sake of minimizing the uncertainties with respect to the reaction mechanism, a large fraction of these investigations were done under or close to quasi-elastic kinematics (Bjorken $x = \frac{-q^\mu q_\mu}{2M_N\omega} \approx 1$). These data sets highlight at the same time the success and the limits of the independent-particle-model (IPM) for atomic nuclei [2]. Indeed, after corrections for final-state interactions and Coulomb distortions of the electron probe, the shape of the deduced proton momentum distributions are systematically in line with the predictions of modern formulations of the nuclear IPM. On the other hand, below the Fermi momentum the absolute magnitude of the deduced momentum distributions are systematically, i.e. independent of the nucleon momentum, lower than IPM predictions. To cut a long story short, the major conclusion from this world-wide $(e, e'p)$ effort seems that an appropriate non-relativistic picture of the nucleus is roughly compatible with 70% *mean-field behaviour* and 30% *“correlations”* an observation which is still frequently ignored in various nuclear structure calculations and model developments. The energy of the available electron beams with a large duty factor ($\epsilon \leq 1$ GeV) made that most of this aforementioned $(e, e'p)$ work was done at four-momentum transfers of the order $Q^2 = -q^\mu q_\mu \leq 0.2$ (GeV/c)². With the advent of the TJNAF and an upgraded Mainz electron facility higher values of Q^2 come into reach of experimental exploration.

Amongst the major physics' goals motivating exclusive $(e, e'p)$ measurements from finite nuclei at higher momentum transfer ($Q^2 \geq 0.2$ (GeV/c)²) one can mention the following ones. The higher Q^2 conditions and unmistakably smaller distance scales probed should make it feasible to achieve a better understanding of the short-range mechanisms in nuclei. At the same time, one could hope to find experimental evidence for the onset of quark and gluon degrees of freedom. Presumably, the most convincing evidence pointing into that direction could come from measurements for processes that are fairly well understood at lower Q^2 (like $(e, e'p)$ at $x=1$) and turn out to be completely at odds with meson/baryon models when higher Q^2 regimes are entered. Another challenge for $(e, e'p)$ measurements at higher momentum transfers is the question whether available relativistic models can succeed in producing a better agreement with the data sets than the non-relativistic ones and if so, which dynamical degrees of freedom make them to be substantially different from what is commonly implemented in the non-relativistic nuclear many-body models. Another fundamental question that has received a great share of attention for many years, is the question whether the nucleon properties (like electromagnetic form factors e.g.) are modified in the nuclear medium. This information is of unvaluable importance for models that embark on the ambitious program of understanding nuclei in terms of quark and gluon degrees of freedom [3,4]. A challenging but at the same time rather ambiguity-free way of probing the medium-dependent form factors, are double polarization observables from $A(\vec{e}, e'\vec{p})$ measurements [5–8]. Indeed, double polarization observables are conceived to be rather insensitive to ambiguities with respect to the final state interactions (FSI) that affect most of the other $A(e, e'p)$ observables. Other effects that are recognized to possibly

*E-mail : jan.ryckebusch@rug.ac.be

complicate the interpretation of double polarization observables in terms of medium-dependent nucleon form factors are gauge ambiguities, channel-couplings and two-body current effects. Whereas the first two sources of possible dilutions were extensively studied by Kelly [9,10] and found to produce very small corrections, the two-body current effects are not well studied for finite nuclei.

Earlier efforts to study the role of two-nucleon currents in exclusive $A(e, e'p)$ reactions from finite nuclei ($A \geq 4$) include the pioneering work of Suzuki [11], the systematic investigations by the Pavia group [12–14] and the ${}^4\text{He}(e, e'p)$ studies as e.g. reported in Refs. [15,5]. In order to make their calculations computationally more attractive, the results of the Pavia group were obtained with a two-body current operator that was formally reduced to an effective one-body one. This approximation adopts a Fermi-gas picture for the residual nucleus that allows to integrate out the coordinates of the second nucleon that gets involved in the photoabsorption process. For the work presented here, we treat the two-body currents in their full (non-relativistic) complexity and deal with the multi-dimensional integrals that automatically occur when several nucleons get involved in the (virtual) photoabsorption process. A similar sort of exact treatment was earlier adopted in our work reported in References [16,17]. There it was found that the effect of the two-body currents on the $A(e, e'p)$ cross sections, just as the role of the coupled-channel effects, is gradually decreasing with increasing momentum transfer. This conforms to the findings with respect to the momentum-transfer dependence of the two-body current effects in the $d(e, e'p)n$ and ${}^4\text{He}(e, e'p)$ [5]. Nevertheless, even at the highest momentum transfer considered in Ref. [16] ($q=600$ MeV/c) the cross sections were predicted to be substantially affected by the two-body currents. In this work the role of meson-exchange and isobar degrees of freedom in $A(\vec{e}, e'\vec{p})$ and $A(e, e'n)$ is investigated in a wide range of four-momentum transfers ($0.2 \leq Q^2 \leq 0.8$ (GeV/c) 2). Special emphasis is placed on the recoil polarization observables as they open perspectives to investigate possible medium modifications of the nucleon properties.

The calculational framework will be introduced in Section II. In Section II A the adopted conventions for the $(\vec{e}, e'\vec{p})$ observables will be introduced. The model for the bound and scattering states is described in Section II B. In Section II C the model assumptions with respect to the one- and two-body current operators will be summarized. The results of the calculations are contained in Section III. Our conclusions are summarized in Section IV.

II. THEORETICAL FRAMEWORK

A. $A(\vec{e}, e'\vec{p})$ observables and kinematics

We consider processes in which a longitudinally polarized electron impinges on a nucleus and induces the following reaction

$$A + \vec{e}(\epsilon) \longrightarrow (A-1)(E_{A-1}, \vec{p}_{A-1}) + N(E_N, \vec{p}_N) + e(\epsilon'), \quad (1)$$

to occur. For such a process the cross section reads in the one photon exchange approximation

$$\frac{d^5\sigma}{d\Omega_N d\epsilon' d\Omega_{e'}}(\vec{e}, e'N) = \frac{1}{4(2\pi)^5} p_N E_N f_{rec}^{-1} \sigma_M \times \left[v_T W_T + v_L W_L + v_{LT} W_{LT} + v_{TT} W_{TT} + h \left[v'_{LT} W'_{LT} + v'_{TT} W'_{TT} \right] \right], \quad (2)$$

where f_{rec} is the recoil factor

$$f_{rec} = \left| 1 + \frac{E_N}{E_{A-1}} \left(1 - \frac{\vec{q} \cdot \vec{p}_N}{p_N^2} \right) \right|, \quad (3)$$

and σ_M the Mott cross section

$$\sigma_M = \frac{\alpha^2 \cos^2 \frac{\theta_e}{2}}{4\epsilon^2 \sin^4 \frac{\theta_e}{2}}. \quad (4)$$

The electron kinematics is contained in the kinematical factors

$$v_T = tg^2 \frac{\theta_e}{2} - \frac{1}{2} \left(\frac{q_\mu q^\mu}{\bar{q}^2} \right) \quad (5)$$

$$v_L = \left(\frac{q_\mu}{\bar{q}} \right)^4 \quad (6)$$

$$v_{LT} = \frac{q_\mu q^\mu}{\sqrt{2} |\bar{q}|^3} (\epsilon + \epsilon') tg \frac{\theta_e}{2} \quad (7)$$

$$v_{TT} = \frac{q_\mu q^\mu}{2\bar{q}^2} \quad (8)$$

$$v'_{LT} = \frac{q_\mu q^\mu}{\sqrt{2}\bar{q}^2} tg \frac{\theta_e}{2} \quad (9)$$

$$v'_{TT} = \sqrt{\left(-\frac{q_\mu q^\mu}{\bar{q}^2} + tg^2 \frac{\theta_e}{2} \right)} tg \frac{\theta_e}{2}, \quad (10)$$

whereas the structure functions are defined in the standard fashion

$$\begin{aligned} W_L &= \left(J_0^{fi} \right)^* \left(J_0^{fi} \right) & W_T &= \left(J_{+1}^{fi} \right)^* \left(J_{+1}^{fi} \right) + \left(J_{-1}^{fi} \right)^* \left(J_{-1}^{fi} \right) \\ W_{LT} &= 2\mathcal{R}e \left[\left(J_0^{fi} \right)^* \left(J_{-1}^{fi} \right) - \left(J_0^{fi} \right)^* \left(J_{+1}^{fi} \right) \right] & W_{TT} &= 2\mathcal{R}e \left[\left(J_{-1}^{fi} \right)^* \left(J_{+1}^{fi} \right) \right] \\ W'_{LT} &= -2\mathcal{R}e \left[\left(J_0^{fi} \right)^* \left(J_{+1}^{fi} \right) + \left(J_0^{fi} \right)^* \left(J_{-1}^{fi} \right) \right] & W'_{TT} &= \left(J_{+1}^{fi} \right)^* \left(J_{+1}^{fi} \right) - \left(J_{-1}^{fi} \right)^* \left(J_{-1}^{fi} \right). \end{aligned} \quad (11)$$

The above definitions for the structure functions and the kinematical variables correspond with those of Ref. [18]. We remind that apart from a negligible parity-violating component, the structure function W'_{TT} vanishes identically and the W'_{LT} in coplanar kinematics if no recoil polarization is determined. A new set of observables comes into reach of experimental exploration when performing polarimetry on the ejected hadron. This results in knowledge about the spin orientation of the ejectile and as e.g. illustrated in neutron form factor studies represents a powerful tool to address fundamental physical quantities. The formal framework for the electroproduction of polarized nucleons from nuclei is outlined in great detail in Refs. [18–20] and will not be repeated here. Here, we only review some basic concepts which mainly serves at introducing the conventions adopted. For the results presented below, the polarization of the escaping nucleon is expressed in the so-called barycentric reference frame that is defined by the following set of unit vectors (Fig. 1)

$$\begin{aligned} \hat{l} &= \frac{\vec{p}_N}{|\vec{p}_N|} \\ \hat{n} &= \frac{\vec{q} \times \vec{p}_N}{|\vec{q} \times \vec{p}_N|} \\ \hat{t} &= \hat{n} \times \hat{l}. \end{aligned} \quad (12)$$

Note that for coplanar kinematics \hat{n} determines the y axis of the reference frame. The escaping nucleon polarization observables can be determined through measuring **ratios**. The *induced polarization* can be addressed with unpolarized electrons (i=n,l,t)

$$P_i = \frac{\sigma(s_N^i = \uparrow) - \sigma(s_N^i = \downarrow)}{\sigma(s_N^i = \uparrow) + \sigma(s_N^i = \downarrow)}, \quad (13)$$

whereas the *polarization transfer* also requires polarized electron beams (i=n,l,t)

$$P'_i = \frac{[\sigma(h = 1, s_N^i = \uparrow) - \sigma(h = -1, s_N^i = \uparrow)] - [\sigma(h = 1, s_N^i = \downarrow) - \sigma(h = -1, s_N^i = \downarrow)]}{[\sigma(h = 1, s_N^i = \uparrow) + \sigma(h = -1, s_N^i = \uparrow)] + [\sigma(h = 1, s_N^i = \downarrow) + \sigma(h = -1, s_N^i = \downarrow)]}, \quad (14)$$

where $s_N^i = \uparrow$ denotes that the ejected hadron is spin-polarized in the positive i direction (i=(n,l,t)) and h is the helicity of the electron impinging on the target nucleus. $\sigma(h, s_N^i)$ is a shorthand notation for the differential cross section for an electrodisintegration process initiated by an electron with helicity h and for which the ejectile is detected with a spin polarization characterized by s_N^i . Throughout this work we adopt relativistic kinematics.

B. Final-state interactions

For the model calculations presented here, the bound and scattering states are produced by solving a Schrödinger equation with a mean-field potential that is obtained from a Hartree-Fock calculation. The latter are performed with an effective nucleon-nucleon force of the Skyrme type. The mean-field potential includes central, spin-orbit and Coulomb terms. This model does not require any empirical input with respect to the initial and final-state potentials. Moreover, the orthogonality condition between the initial and final states is obeyed and gauge invariance is preserved at the one-body current level. A drawback of the model is that the inelastic processes, which are commonly accounted for through imaginary parts in the final-state potential, are only partially included. The major impact of the rescattering processes in exclusive ($e, e'p$) is generally conceived, however, to be a mere reduction of the absolute cross section. In the kinematics regime of interest here, the reduction factor can be estimated from nuclear transparency ($e, e'p$) measurements as they were recently performed at TJNAF for various target nuclei [21].

The differential cross section, the various structure functions and polarization observables are all calculated starting from the following set of transition matrix elements

$$m_{\lambda}^{fi} = \langle J_R M_R(E_x); \vec{p}_N, \frac{1}{2} s_N^z | J_{\lambda}(q) | J_i M_i \rangle \quad (\lambda = 0, \pm 1) \quad (15)$$

where $|J_i M_i\rangle$ and $|J_R M_R(E_x)\rangle$ refer to the quantum states of the target and residual A-1 nucleus and s_N^z denotes the spin projection of the ejectile along the z-axis. The latter is chosen to coincide with the direction of the momentum transfer \vec{q} . When calculating the induced and transverse polarizations as defined in Eqs. (13) and (14) the transition matrix element for the ejectile's spin pointing in a certain direction determined by the polar and azimuthal angle (θ^*, ϕ^*) are required. These can be easily obtained from the above matrix elements (15) by remarking that

$$\begin{aligned} & \langle J_R M_R(E_x) \vec{p}_N, \frac{1}{2} s'_N(\theta^* \phi^*) | J_{\lambda}(q) | J_i M_i \rangle = \\ & \sum_{s_N^z} \left(\mathcal{D}_{s_N^z, s'_N}^{(1/2)}(\theta^*, \phi^*) \right)^* \langle J_R M_R(E_x); \vec{p}_N, \frac{1}{2} s_N^z | J_{\lambda}(q) | J_i M_i \rangle \quad (\lambda = 0, \pm 1), \end{aligned} \quad (16)$$

where $\mathcal{D}^{(1/2)}$ is the Wigner \mathcal{D} -matrix for $j = \frac{1}{2}$

$$\mathcal{D}^{(1/2)}(\theta^*, \phi^*) = \begin{pmatrix} \cos \frac{\theta^*}{2} & \sin \frac{\theta^*}{2} e^{i\phi^*} \\ \sin \frac{\theta^*}{2} & -\cos \frac{\theta^*}{2} e^{i\phi^*} \end{pmatrix}. \quad (17)$$

In determining the matrix elements of Eq. (15), a standard multipole expansion for the electromagnetic current operators and the “distorted” outgoing nucleon wave is made. The multipole expansion of the current operators tends to converge more slowly as more extended systems and higher momentum transfers are addressed. For the highest momentum transfer considered here ($|\vec{q}| \approx 1$ GeV), convergence in the ^{16}O calculations could only be reached after including all multipolarities up to $J_{max}=30$. This number is compatible with the estimate one would obtain by setting $J_{max} = 2qR_A$, where R_A is the nuclear radius determined by $R_A = 1.2 A^{1/3}$ (fm). The large number of multipoles required for calculations at high momentum transfer is a serious numerical complication that prevents models that were developed for lower energy and momentum transfers from being easily extended to higher energy and momentum domains. Apart from the fact that a full treatment of the relativistic effects would be in order, the partial-wave expansion technique hampers extending the presented formalism beyond the range of momentum-transfers considered here ($|\vec{q}| \leq 1$ GeV/c).

A quasi-elastic ($e, e'p$) process will predominantly excite those A-1 states $|J_R M_R(E_x)\rangle$ that bear a sizeable hole state component in their overlap with the ground-state of the target nucleus. This component of the final wave function can be constructed starting from the standard multipole expansion in terms of particle-hole $|p(lj\epsilon)h^{-1}\rangle$ excitations out of the ground state of the target nucleus [22,23]:

$$\begin{aligned} \left| J_R M_R(E_x); \vec{p}_N, \frac{1}{2} s_N^z \right\rangle &= \sum_{l m_l} \sum_{j m} 4\pi i^l \sqrt{\frac{\pi}{2\mu p_N}} \langle j_h m_h j m | J M \rangle \\ &\times \langle l m_l \frac{1}{2} s_N^z | j m \rangle e^{i(\delta_l + \sigma_l)} Y_{l m_l}^*(\Omega_N) | p(lj\epsilon)h^{-1}; J M \rangle, \end{aligned} \quad (18)$$

where $\epsilon \equiv p_N^2/(2\mu)$, μ is the reduced mass of the outgoing nucleon, δ_l is the central phase shift and σ_l is the Coulomb phase shift related to the electromagnetic part of the mean-field potential. The above expression has been derived for

the following conventions with respect to the asymptotic behaviour of the continuum eigenstates $|p(lj\epsilon)\rangle \equiv \varphi_{lj}(r, E)$ of the mean-field potential and the total A-body wave function:

$$\varphi_{lj}(r, \epsilon) \xrightarrow{r \gg R_A} \sqrt{\frac{2\mu}{\pi p_N}} \frac{\sin(p_N r - \eta \ln(2p_N r) - \frac{\pi l}{2} + \delta_l + \sigma_l)}{r},$$

$$\left| J_{RM} M_R(E_x); \vec{p}_N, \frac{1}{2} s_N^z \right\rangle \xrightarrow{r_A \gg R_A} \frac{1}{\sqrt{A}} \left(e^{i\vec{p}_N \cdot \vec{r}_A} + f_k(\theta) \frac{e^{ip_N r_A}}{r_A} \right) \left| \frac{1}{2} s_N^z \right\rangle (-1)^{j_h+m_h} c_{h-m_h} | J_i M_i \rangle, \quad (19)$$

where R_A is the nuclear radius.

C. One and Two-body current operators

The one-body current is derived from the on-shell covariant single-nucleon current

$$j^\mu = \bar{u}(\vec{p}_N, s_N^z) \left[F_1(Q^2) \gamma^\mu + F_2(Q^2) \frac{i\sigma^{\mu\nu} q_\nu}{2M_N} \right] u(\vec{p}_m, s_m^z), \quad (20)$$

where $F_1(F_2)$ is the Dirac (Pauli) form factor. Even when making an abstraction from issues related to off-shell corrections, the derivation of an appropriate current operator with relativistic corrections to be used in calculations that adopt a non-relativistic description for the strong interaction part of the reaction process, is not free from ambiguities [24–27]. For example, the two standard techniques to derive a non-relativistic reduction of relativistic hamiltonians, i.e. the Foldy-Wouthuysen (FW) and the “direct Pauli reduction” method, have been shown to make a difference as far as the final expressions for the current operators are concerned [25]. Admittedly, the problems encountered in implementing relativistic corrections in non-relativistic calculations can be avoided by adopting a fully relativistic description for the nuclear dynamics. Over the years, a number of fully relativistic models for $(e, e'p)$ have been developed [28–31]. Basically, all of these models start from a relativistic formulation of the mean-field idea and do not embody current operators that go beyond the IA. Unfortunately, for finite nuclei a realistic, empirically well-founded and practicable relativistic nuclear-structure model that *also accounts for the multi-nucleon degrees of freedom* is as yet not available. With this in mind we shall resort to a non-relativistic approach for the strong interaction dynamics of the $(e, e'p)$ process. We deem this model to be a reliable and valuable testing ground to estimate the relative importance of subnuclear degrees of freedom. The conventional way of deriving a nonrelativistic reduction of the above one-body current operator is the FW technique which relies on a (q/M_N) expansion. Recently, an alternative expansion in terms of (p_m/M_N) , with p_m the momentum of the nucleon on which the absorption occurs, has been suggested [24,27]. This expansion is based on the “direct Pauli reduction” method. In order $(q/M_N)^2$ and (p_m/M_N) respectively, both methods give rise to a nonrelativistic four-current density operator that reads in coordinate space

$$\rho(\vec{r}) = \sum_{i=1}^A \left(C_1(q, Q^2) G_E^i(Q^2) \delta(\vec{r} - \vec{r}_i) - C_2(q, Q^2) \frac{(2G_M^i(Q^2) - G_E^i(Q^2))}{8M_N^2 i} \vec{\nabla} \cdot [\vec{\sigma}_i \times \{ \vec{\nabla}_i, \delta(\vec{r} - \vec{r}_i) \}] \right)$$

$$\vec{J}^\perp(\vec{r}) = \sum_{i=1}^A C_3(q, Q^2) \left(\frac{G_E^i(Q^2)}{2M_N i} \{ \vec{\nabla}_i, \delta(\vec{r} - \vec{r}_i) \} + \frac{G_M^i(Q^2)}{2M_N} \delta(\vec{r} - \vec{r}_i) (\vec{\sigma}_i \times \vec{\nabla}) \right), \quad (21)$$

where $\{ \dots, \dots \}$ denotes the anticommutator and it is implicitly understood that the operator $\vec{\nabla}$ acts only the photon field. The $G_E(Q^2)$ and $G_M(Q^2)$ are the Sachs form factors for which we have adopted the standard dipole form. The major difference between the current operators in the two earlier sketched approaches is not the operatorial form but the derived expression for the coefficients (C_1, C_2, C_3) . Whereas with the FW method one finds [32]

$$C_1(q, Q^2) = \frac{1}{\sqrt{1 + \frac{Q^2}{4M_N^2}}} \quad C_2(q, Q^2) = 1 \quad C_3(q, Q^2) = 1, \quad (22)$$

a (p_m/M_N) expansion with the aid of the Pauli reduction technique leads to [24,27]

$$C_1(q, Q^2) = \frac{q}{\sqrt{Q^2}} \quad C_2(q, Q^2) = \frac{1}{\sqrt{1 + \frac{Q^2}{4M_N^2}}} \quad C_3(q, Q^2) = \frac{\sqrt{Q^2}}{q}. \quad (23)$$

Unless otherwise specified all results of this paper are obtained with the four-current operator from Eq.(21) using the C coefficients as they are obtained with the FW method. The major difference in comparison with a strict non-relativistic approach is the introduction of a spin-orbit term $\rho^{so}(\vec{r})$ in the charge density operator. This gives rise to a spin-orbit term in the Coulomb transition operator that determines the longitudinal strength

$$M_{JM}^{so}(q) = \int d\vec{r} j_J(qr) Y_{JM}(\Omega) \rho^{so}(\vec{r}). \quad (24)$$

In coordinate space the one-body transition matrix element corresponding with this operator reads

$$\begin{aligned} \left\langle n_a l_a \frac{1}{2} j_a \parallel M_{J'}^{so}(q) \parallel n_b l_b \frac{1}{2} j_b \right\rangle &= \sum_{\eta \pm 1, J_2} (-1)^{\delta_{\eta, -1} + 1} C_2(q, Q^2) \frac{(2G_M(Q^2) - G_E(Q^2))}{8M_N^2} \\ &\times 3\sqrt{12(J + \delta_{\eta, +1})(2J_2 + 1)} \begin{Bmatrix} J_2 & J + \eta & 1 \\ 1 & 1 & J \end{Bmatrix} \begin{Bmatrix} l_a & \frac{1}{2} & j_a \\ l_b & \frac{1}{2} & j_b \\ J_2 & 1 & J \end{Bmatrix} \\ &\times \left\langle n_a l_a \parallel \left(\frac{d}{dr} j_J(qr) + (-1)^{\delta_{\eta, +1}} (J + \delta_{\eta, -1}) \frac{j_J(qr)}{r} \right) \left[Y_{J+\eta} \otimes (\vec{\nabla} - \vec{\nabla}') \right]^{(J_2)} \parallel n_b l_b \right\rangle. \end{aligned} \quad (25)$$

In determining the two-body current operators we start from the observation that of all mesons carrying the nucleon-nucleon interaction the pions play a predominant role. In our model calculations, the current operators that explicitly account for subnuclear π and Δ degrees of freedom are effectively written in terms of the coordinates of the two nucleons involved. The meson-exchange and Δ -isobar currents as they were implemented in our calculations have been discussed in detail in Ref. [33]. The two-body pion-exchange currents are derived from the one-pion exchange potential in the standard fashion. The derivation of the Δ -current operator is somewhat more complicated. Indeed, this operator cannot be constrained through charge-current conservation and is therefore often referred to as a ‘‘model-dependent’’ operator [32]. Moreover, of all pion-related two-body current contributions the Δ -current is the only one that could be unambiguously shown to exhibit a quite strong medium dependence. We do not consider explicit Δ admixtures in the wave functions, so that all isobars in our model calculations are attached to a photon line. In our derivations, the $\pi N\Delta$ and $\gamma N\Delta$ coupling are considered in the standard form :

$$\mathcal{L}_{\pi N\Delta} = \frac{f_{\pi N\Delta}}{m_\pi} \left(\vec{S}^\dagger \cdot \vec{\nabla} \right) \left(\vec{T}^\dagger \cdot \vec{\pi} \right), \quad (26)$$

$$\mathcal{L}_{\gamma N\Delta} = G_{\gamma N\Delta}(q_\mu^2) \frac{f_{\gamma N\Delta}}{m_\pi} \left(\vec{S}^\dagger \times \vec{\nabla} \right) \cdot \vec{A} \vec{T}_z^\dagger, \quad (27)$$

where \vec{S} and \vec{T} denote the $\frac{1}{2} \rightarrow \frac{3}{2}$ spin and isospin transition operators, \vec{A} is the external electromagnetic field and the coupling constants are $\frac{f_{\pi N\Delta}^2}{4\pi} = 0.37$ and $f_{\gamma N\Delta} = 0.12$. The electromagnetic form factor of the delta $G_{\gamma N\Delta}(q_\mu^2)$ is parametrized as [34]

$$G_{\gamma N\Delta}(q_\mu^2) = \frac{1}{\left(1 - \frac{q_\mu^2}{\Lambda_1^2}\right)^2} \frac{1}{\sqrt{1 - \frac{q_\mu^2}{\Lambda_2^2}}}, \quad (28)$$

where $\Lambda_1=0.84$ GeV/c and $\Lambda_2=1.2$ GeV/c. It is interesting to note that the $N - \Delta$ electromagnetic form factor $G_{\gamma N\Delta}$ is decreasing with Q^2 faster than the nucleon dipole form [35,36]. With the above coupling lagrangians we arrive at the following expression for the Δ_{33} -current in momentum space

$$\begin{aligned} \vec{J}_{\pi\Delta}(\vec{q}, \vec{k}_1, \vec{k}_2; \gamma N\Delta \rightarrow NN) &= \frac{i}{9} \frac{f_{\gamma N\Delta} f_{\pi NN} f_{\pi N\Delta}}{m_\pi^3} G_{\gamma N\Delta}(q_\mu^2) \\ &\times \left[(G_\Delta^I + G_\Delta^{II}) \left(4\vec{\tau}_{2,z} \left(\vec{k}_2 \times \vec{q} \right) \frac{\vec{\sigma}_2 \cdot \vec{k}_2}{k_2^2 + m_\pi^2} + 4\vec{\tau}_{1,z} \left(\vec{k}_1 \times \vec{q} \right) \frac{\vec{\sigma}_1 \cdot \vec{k}_1}{k_1^2 + m_\pi^2} \right. \right. \\ &+ \left. \left. (\vec{\tau}_1 \times \vec{\tau}_2)_z \left[\left(\vec{\sigma}_2 \times \vec{k}_1 \right) \frac{\vec{\sigma}_1 \cdot \vec{k}_1}{k_1^2 + m_\pi^2} - \left(\vec{\sigma}_1 \times \vec{k}_2 \right) \frac{\vec{\sigma}_2 \cdot \vec{k}_2}{k_2^2 + m_\pi^2} \right] \times \vec{q} \right) \right. \\ &+ \left. (G_\Delta^I - G_\Delta^{II}) \left(-2i\vec{\tau}_{2,z} \left(\left(\vec{\sigma}_1 \times \vec{k}_2 \right) \times \vec{q} \right) \frac{\vec{\sigma}_2 \cdot \vec{k}_2}{k_2^2 + m_\pi^2} - 2i\vec{\tau}_{1,z} \left(\left(\vec{\sigma}_2 \times \vec{k}_1 \right) \times \vec{q} \right) \frac{\vec{\sigma}_1 \cdot \vec{k}_1}{k_1^2 + m_\pi^2} \right) \right] \end{aligned}$$

$$-2i(\vec{\tau}_1 \times \vec{\tau}_2)_z \left[\vec{k}_2 \frac{\vec{\sigma}_2 \cdot \vec{k}_2}{k_2^2 + m_\pi^2} - \vec{k}_1 \frac{\vec{\sigma}_1 \cdot \vec{k}_1}{k_1^2 + m_\pi^2} \right] \times \vec{q} \quad (29)$$

At the $\pi N \Delta$ and πNN vertices, monopole form factors

$$\frac{\Lambda_{\pi NN}^2 - m_\pi^2}{\Lambda_{\pi NN}^2 + p_\pi^2} \quad (30)$$

are introduced. They correct for finite size effects of the interacting baryons and regularize the πNN interaction at extremely short distances. All results presented below are obtained with a cut-off parameter $\Lambda_{\pi NN}$ of 1250 MeV/c. This value corresponds with those that are typically obtained in the latest parametrizations of the Bonn potential. In the above expression, G_Δ^I (G_Δ^{II}) denotes the propagator for a Δ resonance that is created after (before) photoabsorption. In the calculations we adopt the following propagators

$$G_\Delta^I = \frac{1}{-\sqrt{s_\Delta^I} + M_\Delta - \frac{i}{2}\Gamma_\Delta^{res} + V_\Delta}$$

$$G_\Delta^{II} = \frac{1}{-\sqrt{s_\Delta^{II}} + M_\Delta}, \quad (31)$$

where $\sqrt{s_\Delta}$ is the intrinsically available energy for the resonance, $M_\Delta=1232$ MeV and Γ_Δ^{res} the “free” πN decay width [37,38]

$$\Gamma_\Delta^{res} = \frac{2}{3} \frac{f_{\pi N \Delta}^2}{4\pi} \frac{|\vec{p}_\pi|^3}{m_\pi^2} \frac{M_N}{\sqrt{s_\Delta}}, \quad (32)$$

where \vec{p}_π is the decay momentum in the center-of-mass (c.o.m) frame of the πN system.

As we are dealing with off-shell nucleons the photon energy is not completely available for internal excitation of the Δ_{33} resonance. This effect is partially responsible for the observed (real) energy shift of the Δ in the medium. A reasonable substitution for s_Δ is [39,40]

$$(s_\Delta^I)^2 = -q_\mu q^\mu + (M_N - \epsilon_h)^2 + 2\omega(M_N - \epsilon_h) \quad (33)$$

$$(s_\Delta^{II})^2 = \left(\sqrt{M_N^2 + |\vec{q}|^2} - \omega \right)^2, \quad (34)$$

where ϵ_h is the binding energy of the mean-field orbit on which the pion is reabsorbed. The above expression accounts for the observation that the delta peak in (e, e') spectra section shifts to higher ω 's with increasing momentum transfer.

Various pion-nucleus [41], real photoabsorption [42] and electron scattering studies [43,44] experiments have pointed towards to strong medium modifications of the Δ_{33} resonance. For that reason, a medium-dependent term V_Δ that accounts for the interaction of the Δ resonance with the nucleus was added to the propagator written in (Eq. 31). Various models that implement a dynamical description of isobar propagation in the medium have been developed [43,41]. These models are generally reasonably successful in describing the cross sections for inclusive (e, e') reactions in the Δ_{33} resonance region [44,45]. The medium modifications of the Δ -resonance appear to be better under control in electromagnetically induced processes than for example in pion-absorption reactions [46]. For example, Chen and Lee [47] have shown that a fairly good description of the $^{12}\text{C}(e, e')$ cross sections could be achieved with a Δ propagator of the type as written in Eq. (31) provided that one introduces a simple medium correction of the type $V_\Delta[\text{MeV}] = -30 - 40i$. Similar values for the Δ -mass shift and broadening have been found in other theoretical approaches [48] and were deduced from recent total photoabsorption measurements [42]. For the calculations presented here, we have used the Δ -medium potential V_Δ as it was calculated by Oset and Salcedo [49]. In Figure 3 the imaginary part of V_Δ is shown. In the resonance region, this calculation does indeed reproduce the earlier quoted value for the broadening of the resonance. The above two-body current operators have been used to calculate $^{12}\text{C}(\gamma, pp)$ and $^{12}\text{C}(\gamma, pn)$ total cross sections in the resonance region. Not only could the position and width of the resonance be reasonably reproduced, also the $(\gamma, pp)/(\gamma, pn)$ ratio for the various shell-model orbits agreed fairly well with experiment [50]. These results lend confidence in the model assumptions with respect to the Δ currents and propagators.

Introducing the earlier discussed two-body current operators in exclusive single-nucleon knockout calculations one ends with the diagrams sketched in Figure 2. The diagrams of Figure 2(b),(c) and (d) are the pion-exchange contributions to single-nucleon knockout and necessarily imply a charge-exchange mechanism carried by a charged pion. As a

consequence, for proton knockout the sum over all occupied single-particle states in the target nucleus ($\sum_{h'}$) produces solely non-zero contributions for the neutron states. The diagrams from Figure 2(e)-(h) involve Δ_{33} excitation after interaction of one of the target's nucleons with the (virtual) photon field. For this class of diagrams both charged and neutral pion exchange belongs to the possibilities. The contributions drawn in Figures 2(e) and (h) involve exclusively neutral pion exchange. Finally, the type of processes drawn in Figure 2(i)-(l) involve a pre-formed Δ that is deexcited after interacting with the photon field. Technically speaking, the introduction of the two-body current operators implies that for each combination of a multipole component of the electromagnetic transition operator T_J and a partial wave of the ejectile's wave function ($|p(lj\epsilon)\rangle$), two-body matrix elements of the type

$$\begin{aligned} \langle p(lj\epsilon)h^{-1}; J || T_J^{[2]}(q) || 0^+(g.s.) \rangle = & \sum_{h'J_1J_2} \sqrt{2J_1+1}\sqrt{2J_2+1}(-1)^{j_h-j_{h'}-J-J_2} \begin{Bmatrix} j_h & j_{h'} & J_1 \\ J_2 & J & j \end{Bmatrix} \\ & \times \left(\langle hh' ; J_1 || T_J^{[2]}(q) || p(lj\epsilon)h' ; J_2 \rangle - (-1)^{j_h'+j+J_2} \langle hh' ; J_1 || T_J^{[2]}(q) || h'p(lj\epsilon) ; J_2 \rangle \right), \end{aligned} \quad (35)$$

are to be coherently added to the conventional one-body current contribution from the Impulse Approximation (IA)

$$\langle p(lj\epsilon)h^{-1}; J || T_J^{[1]}(q) || 0^+(g.s.) \rangle . \quad (36)$$

In the above expression, $T_J^{[1]}$ and $T_J^{[2]}$ is the one and two-body current contribution to the electromagnetic transition operator. The explicit expressions for the reduced two-body matrix elements with the meson-exchange and isobar currents can be found in Refs. [33,51]. The sum over h' involves all occupied proton and neutron single-particle states. It speaks for itself that for a nucleus like ^{208}Pb this summation can only be performed at a large computational cost. For consistency reasons and to avoid orthogonality deficiencies, the wave functions for all occupied states h' are calculated in exactly the same mean-field potential in which also the distorted outgoing nucleon wave and the overlap wave function $\langle J_R M_R(E_x) | J_i M_i \rangle$ is determined. We remark that the very same type of matrix elements that dictate the two-body current contributions to the single-nucleon knockout processes, determine the two-body current contributions to the cross sections for the $A(\gamma, NN)$ and $A(e, e'NN)$ processes that are presently the subject of investigation at various laboratories. It speaks for itself that two-nucleon knockout processes represent an intrinsically superior way of exploring the two-nucleon effects in nuclei. The model assumptions with respect to the current operators adopted here, are identical to those that we have adopted in our two-nucleon knockout studies. Also the potential in which the bound and scattering states are calculated are identical for the single- and two-nucleon knockout studies. To illustrate the potential of two-nucleon knockout studies to acquire a precise understanding of two-nucleon mechanisms in finite systems, Figure 4 shows a comparison of recently obtained $^{16}\text{O}(e, e'pp)$ data and our model calculations for the three lowest bins in the excitation energy spectrum in ^{14}C . The comparison between the calculations and the data is done as a function of the pair missing momentum $|\vec{P}| = |\vec{p}_1 + \vec{p}_2 - \vec{q}|$, which is the c.m. momentum of the pair before it undergoes the electromagnetic interaction with the photon field and is established to be the scaling variable in two-nucleon knockout processes, i.e. the counterpart of the variable $|\vec{p}_m| = |\vec{p}_N - \vec{q}|$ in the $(e, e'p)$. For the data shown in Figure 4 the experimental resolution in the excitation (or missing) energy of ^{14}C was of the order of 4 MeV and the individual states could not be resolved in the missing energy spectrum. On the other hand, high-resolution $^{16}\text{O}(e, e'pp)$ investigations from Mainz [52] and $^{15}\text{N}(d, ^3\text{He})^{14}\text{C}$ transfer reactions [53] allow to infer that the lowest excitation-energy bin ($-4 \text{ MeV} \leq E_x \leq 4 \text{ MeV}$) is exclusively fed through the ^{14}C ground-state transition, whereas the second ($4 \text{ MeV} \leq E_x \leq 9 \text{ MeV}$) and third bin ($9 \text{ MeV} \leq E_x \leq 14 \text{ MeV}$) are mainly fed through the $|2^+; E_x = 7.01, 8.32 \text{ MeV}\rangle$ doublet and the $|1^+; E_x = 11.3 \text{ MeV}\rangle$ state respectively. These states can be safely quoted to be the only ones in the low excitation-energy spectrum of ^{14}C that have a dominant “two-hole” structure relative to the ground state of ^{16}O . This information allows to constrain the nuclear-structure input that is required for the $(e, e'pp)$ calculations. The overall agreement between the calculations, that are parameter-free, and the data is reasonable and lends support for the model assumptions with respect to the Δ -current operator and propagator. Indeed, for the transitions to the 2^+ and 1^+ states intermediate Δ creation is predicted to be the dominant reaction process in the $(e, e'pp)$ reaction under evaluation. The shaded region in Figure 4 is the calculated contribution from the central Jastrow correlations to the two-proton knockout cross sections. They make a big contribution to the ground-state transition (upper panel) in the low missing momentum regime $P \leq 250 \text{ MeV}/c$ which can be inferred to arise from diproton knockout from heavily correlated $^1S_0(T=0)$ pairs [54]. For the results presented in Figure 4 the contribution from the Jastrow or short-range correlations (SRC) was calculated with a correlation function as it was obtained from a G-matrix calculation by Gearhart and Dickhoff [55]. Recently, this correlation function was shown to produce a favorable agreement with $^{12}\text{C}(e, e'pp)$ data [56]. In comparison with other model predictions for the central correlation function, the one obtained by Gearhart and Dickhoff should be classified in between the categories of “hard” (with a core at short internucleon distances) and “soft” (characterized by a finite probability to observe nucleon pairs at very short internucleon distances).

III. RESULTS AND DISCUSSION

A. $^{16}\text{O}(\bar{e}, e'\bar{p})$ and $^{12}\text{C}(\bar{e}, e'\bar{p})$ results for $0.05 \leq Q^2 \leq 0.50$ (GeV/c)²

We start our investigations into the role of two-currents for the kinematics of an $^{16}\text{O}(e, e'p)$ experiment made at MAINZ and reported in Reference [57]. In this experiment, the cross sections were measured in a broad missing momentum range between 100 and 700 MeV/c. The data were compared to distorted wave impulse approximation (DWIA) calculations. At lower missing momenta ($p_m \leq 300$ MeV/c) the data were observed to overshoot these calculations by a factor of two, whereas for the highest missing momenta probed the opposite effect was noticed. This qualitative behaviour was recently confirmed in an independent calculation by J.J. Kelly [9]. Despite the fact that rather large bound nucleon momenta were probed it was concluded that the deviations from standard (Woods-Saxon) mean-field wave functions are modest. This observation lends support for the picture that nucleon-nucleon correlations are related to the hard-core part of the nucleon-nucleon interaction and are not expected to bring about large deviations from mean-field models in single-knockout processes as long as low excitation energies in the A-1 system are probed. The data of Ref. [57] were obtained for an initial electron energy of 855.1 MeV and $T_p \approx 195$ MeV. As a large fraction of the data were taken in parallel kinematics ($\vec{q} \parallel \vec{p}_N$), the momentum transfer had to be decreased as higher missing momenta were probed. Consequently, to reach higher missing momenta one had to move out of quasi-elastic kinematics. Figures 5 and 6 show the predicted sensitivity of the Mainz results to the two-body currents. The Figures show results for four different central values in Q^2 and parallel kinematics. The kinematics is such that one moves out of quasi-elastic conditions as higher missing momenta are probed. As is commonly done, we present the angular cross-sections in terms of the reduced cross section “ ρ_m ”. Hereby, we adopt the standard convention of dividing the calculated cross sections by a kinematical factor times the so-called “CC1” [58] elementary electron-proton cross section

$$\rho_m \equiv \frac{\frac{d^5\sigma}{d\Omega_N d\epsilon' d\Omega_{e'}}}{\frac{p_N E_N}{(2\pi)^3} f_{rec}^{-1} \sigma_{ep}^{CC1}}. \quad (37)$$

Referring to Figures 5 and 6, striking features are: (1) the sensitivity of the cross sections to the two-body currents is substantial and (2) the two-body currents do not dramatically alter the shape of the reduced cross section for none of the four Q^2 values considered. As a consequence, the impact of the two-body currents would generally not be noticed when comparing results of calculations performed within the IA with data but would simply be “effectively” accounted for in the spectroscopic factor that is used to scale the DWIA calculations to the data. The net effect of the two-body currents is a reduction of the cross sections. This reduction is of the order 10-20% for the lowest missing momenta range and can amount to a factor of two at $p_m \approx 300$ MeV/c. Note that for the highest missing momenta considered in Figures 5 and 6 inclusion of the two-body currents tends to increase the cross section. This is generally the case when higher missing momenta are probed [59]. The observed reduction at low missing momenta that was ascribed to two-body current effects is not sufficient to explain why the data are substantially lower (factor of two) than expected on the basis of DWIA models. Indeed, the curves of Figures 5 and 6 are obtained with a reduction factor of 0.25 for the ground-state transition and 0.30 for the $^{16}\text{O}(e, e'p)^{15}\text{N}(3/2^-, 6.32 \text{ MeV})$ transition. With these values we obtain reasonable visual fits of the data. The transparency at the considered four-momentum transfers Q^2 is experimentally determined to be about 0.75 for a light nucleus like ^{12}C [21,60]. When correcting the reduction factors we have applied to obtain visual fits of the data, for transparency (or attenuation) corrections that fall beyond the scope of our model calculations, we obtain the spectroscopic factors $S_{lj}(1/2^-, E_x=0.0 \text{ MeV}) \approx 0.67$ and $S_{lj}(3/2^-, E_x=6.3 \text{ MeV}) \approx 1.6$. In line with the theoretical conclusions drawn from the analyses of References [57] and [10] these values are substantially smaller than the values obtained with high-resolution measurements at lower proton kinetic energies where it was found that $S_{lj}(1/2^-, E_x=0.0 \text{ MeV})=1.20$ and $S_{lj}(3/2^-, E_x=6.3 \text{ MeV})=2.00$ [61]. Note, however, that for $1p_{3/2}$ knockout the spectroscopic factor that is deduced from the calculations that include the two-body currents is about 30% larger than the value that would be deduced in the IA.

Another striking feature of the results displayed in Figures 5 and 6 is that the influence of the subnuclear degrees-of-freedom is more pronounced for knockout from the “stretched” ($j_h = l_h + \frac{1}{2}$) orbit (i.e. $1p_{3/2}$) than from its “jack-knifed” spin-orbit partner ($j_h = l_h - \frac{1}{2}$) (i.e. $1p_{1/2}$). The major reason for this behaviour is simply that all the two-body current operators have a strong spin dependency. It is worth mentioning that the relativistic effects arising from the lower (or negative energy) components in the bound state wave functions were recently shown to have a similar sort of sensitivity. Indeed, the (relativistic) $(e, e'p)$ results for knockout from the “stretched” orbits will be closer to their respective non-relativistic limits than those for “jack-knifed” orbits [62]. Accordingly, the predicted relativistic effects attributed to the small components in the bound state wave functions are smallest for these transitions with maximal two-body current contributions.

The question arises whether the relatively strong sensitivity to two-body currents noticed in Figures 5 and 6 is an intrinsic property of the specific Q^2 range probed or is rather due to the fact that these results were acquired at smaller values of x and subsequently clearly out of quasi-elastic conditions. Results for real quasi-elastic kinematics at about the same value for the proton's kinetic energy and initial electron energy are shown in Figures 7. These results are obtained in quasi-perpendicular kinematics. Here, the variation in missing momentum is reached by varying the polar angle θ_p of the ejected proton. For the remainder of this paper all calculated (reduced) cross sections are shown for full sub-shell occupancy, i.e. $S_{lj} = (2j + 1)$. It becomes clear that under strict quasi-elastic conditions the effect of the subnuclear degrees-of-freedom is substantially smaller than at smaller values of Bjorken x . It is worth mentioning that the results of Figure 7 are obtained in more transverse kinematics than those of Figures 5 and 6. Accordingly, with the eye on minimizing the effect of two-body currents it is very essential to move in quasi-elastic conditions *even if this implies shifting to kinematics which is conceived to be transverse*. Another observation is that the extent to which the two-body currents are important does not depend on the polar angle θ_N of the ejected nucleon. Figures 8 and 9 show the structure functions and polarization observables for the same kinematics in which the cross sections of Figure 7 are obtained. In presenting the structure functions we prefer not to divide out any kinematical variables from the different contributions to the total angular cross section. Formally, this means that we write Eq. (2) in the form

$$\frac{d^5\sigma}{d\Omega_N d\epsilon' d\Omega_{\epsilon'}} \equiv \sigma_L + \sigma_T + \sigma_{LT} + \sigma_{TT} + h(\sigma'_{LT} + \sigma'_{TT}) , \quad (38)$$

where the precise definition of all contributing terms is obvious. This way of presenting results has the outspoken advantage that the relative contribution of each term in the cross section can be easily evaluated. Furthermore, possible confusions regarding the adopted definitions for the different structure functions are avoided. In line with the observations made for ^4He and the deuteron [63] case, the interference terms that are an order of magnitude smaller than σ_L and σ_T exhibit the strongest sensitivity to contributions that go beyond the IA.

We now turn to the discussion of the recoil polarization observables. For coplanar kinematics the sole non-vanishing recoil polarization observables are P_n, P'_l and P'_t . The P_n does vanish identically in the plane-wave impulse approximation. As such it allows to constrain the model assumptions with respect to the final-state interaction (FSI). Inspecting Figure 9 it is clear that at low missing momenta the qualitative behaviour of the induced polarization P_n turns out to be relatively insensitive to the current contributions beyond the impulse approximation. This result confirms the findings of the Pavia calculations reported in Ref. [64]. The first data set for the induced polarization in finite nuclei has recently become available [65]. In Figure 10 the calculated reduced cross section and recoil polarization observables are shown for the kinematics of this experiment. For knockout from the $1s$ shell, where the nucleon is mainly located at high nuclear densities, the influence of the subnuclear d.o.f. is more pronounced than for p -shell knockout. Given that we do not rely on any empirical input for the description of the FSI, the agreement with the data is satisfactory but inferior to the quality of agreement that was reached with the calculations by J.J. Kelly [65]. These calculations constrain the description of the final-state interactions with the aid of optical potentials derived from the analysis of hadronic induced reactions. For most observables, the meson-exchange and isobar effects are acting in opposite directions. At low missing momenta the induced polarization exhibits a small sensitivity to the two-body currents. At moderate and high missing momenta the P_n is predicted to exhibit a large sensitivity to two-body currents. A similar observation is made for the polarization transfer observables. Recently it was shown that the recoil proton polarizations for $p(\vec{\epsilon}, \epsilon' \vec{p})$ and $d(\vec{\epsilon}, \epsilon' \vec{p})n$ are almost identical [66]. From the theory side, rather small contributions from the MEC and IC in the double polarization observables were predicted in the deuteron [63] and ^4He [5] case in quasi-elastic kinematics. Despite the fact that the polarization transfer variable P'_l and P'_t are related to the interference structure functions W'_{TT} and W'_{LT} their predicted sensitivity to the two-body currents looks relatively small. Recently, the polarization transfer observables raised considerable interest in that they would provide a direct handle on the (possible) medium dependence of the nucleon form factors. Indeed, in the plane-wave impulse approximation (PWIA) it can be shown that for electroexcitation from a free proton

$$\frac{P'_l}{P'_t} = -\frac{G_M^p}{G_E^p} \frac{(\epsilon + \epsilon') \tan \frac{\theta_{\epsilon'}}{2}}{2M_p} . \quad (39)$$

It is of the utmost importance to investigate all possible mechanisms that could bring about changes in the above ratio without being related to medium modifications of the form factors. Whereas it was recently shown that final-state interaction and gauge ambiguities effects are only marginally affecting the ratio $\frac{P'_l}{P'_t}$ [67] the question arises whether meson-exchange and isobaric currents could bring about any change in the ratio of the double polarization observables. Whereas the impact of the subnuclear d.o.f. on the value of polarization observables looks small in quasi-elastic kinematics and small missing momenta, the MEC and IC are not necessarily unimportant, especially for

such delicate issues like nucleon form factor studies where the medium dependency is predicted to be modest [4] and the projected accuracy of the planned experiments is astounding. With the aim of studying the sensitivity of the ratio $\frac{P'_t}{P'_i}$ to meson-exchange currents and intermediate isobar creation we have calculated the following double ratio

$$\frac{\left(\frac{P'_t}{P'_i}\right)}{\left(\frac{P'_t}{P'_i}\right)^{IA}} \quad (40)$$

where “IA” refers to the calculated ratio in the impulse approximation, this is when retaining solely the one-body currents in the calculations but keeping all other ingredients fixed. As could be expected, the observed deviation from the IA result enhances as the missing momentum increases. The most favorable regime to perform the recoil polarization measurements for knockout from p-shell orbits, is probably in the peak of the cross section ($p_m \approx 100$ MeV/c). For the $^{16}\text{O}(e, e'p)^{15}\text{N}(1/2^-)$ transition, the deviation in the ratio $\frac{P'_t}{P'_i}$ that is attributed to the MEC and IC is about 5-10% in the peak of the cross section. For knockout from its spin-orbit partner ($1p_{3/2}$) the calculated effect is 10-15%. In both cases, at 200 MeV/c the modifications in the ratio due to two-body currents has grown to 20% and with increasing p_m the effect appears to be rather out of control.

B. $^{16}\text{O}(\vec{e}, e'\vec{p})$ results at $Q^2=0.8$ (GeV/c) 2 and $x \approx 1$

We continue our investigations into the role of two-body currents by considering the kinematics of the TJNAF experiments E89-003 and E8-9033 [6]. The E89-003 experiment has measured the separated structure functions and momentum distributions for $^{16}\text{O}(e, e'p)$ under quasi-elastic conditions at $\epsilon=2.445$ GeV, $\omega=445$ MeV and $q=1$ GeV/c. In E89-033 on the other hand, the $^{16}\text{O}(\vec{e}, e'\vec{p})$ polarization observables were measured for approximately the same kinematics. Figures 11-16 summarize the calculated results for the reduced cross sections, structure functions and recoil polarization observables for knockout from the two p -shell and the s -shell state. In comparing these results with those obtained in the previous Subsection for quasi-elastic conditions at lower four-momentum transfer, we can study the Q^2 dependency of the meson and isobar degrees of freedom. In analogy with the observations made at lower Q^2 , the pion-exchange currents (“MEC”) increase the cross section and this effect is completely counterbalanced by the Δ current that produces the largest contributions. The Q^2 dependency of the two-body current effects can maybe be better estimated from the individual structure functions. Comparing Figures 8 and 13 one does indeed observe a decreasing trend in the relative importance of the two-body currents. A similar tendency is observed for the recoil polarization observables (Figure 15). The deviation in the ratio $\frac{P'_t}{P'_i}$ in the peak of the cross section is of the order of a few percent for the ground-state transition (knockout from the $1p_{1/2}$ orbit), whereas for the excitation of the $3/2^-$ hole state at 6.32 MeV excitation energy in ^{15}N (knockout from the stretched $1p_{3/2}$ orbit) the effect is close to 10%.

With the aim of studying the medium-dependent effects one could be tempted to probe the region of highest nuclear density which for a nucleus like ^{16}O implies studying the region of $1s_{1/2}$ knockout. In light of the mass-independence of the two-body current effects that is frequently alluded to, our findings for $1s_{1/2}$ -knockout in ^{16}O can to a certain extent serve as a guideline for the effects than could be expected in ^4He . From all orbits studied here, knockout from the $1s_{1/2}$ orbit exhibits the strongest sensitivity to the two-body currents. After all, this observation is not that surprising given its stretched status and the fact that the region of highest nuclear density is probed. For example, the LT and TT interference responses in Figure 14 grow substantially after including the two-body currents. Indications for the strong sensitivity of the LT structure function to two-body currents was reported for the ^4He case in Ref. [15]. Also for the recoil polarization observables in the missing-energy range of $1s_{1/2}$ knockout (Figure 16), sizeable contributions from the meson-exchange and isobar currents are predicted. For the ratio $\frac{P'_t}{P'_i}$ the two-body currents bring about a reduction which is slightly bigger than 10%. This is qualitatively very similar with the result obtained for the “stretched” p-shell state ($1p_{3/2}$) (Figure 15) so that some general qualitative behaviour for the sensitivity of the $\frac{P'_t}{P'_i}$ ratio to multi-nucleon currents seems to emerge. Indeed, at low missing momenta and quasi-elastic conditions the two-body currents reduce the ratio $\frac{P'_t}{P'_i}$, an effect that slowly decreases as one goes to higher Q^2 and is larger for knockout from “stretched” than from the “jack-knifed” single-particle orbits. Finally we turn our attention to the role of the relativistic corrections (Section II C) in the one-body current operator. The dotted lines in Figures 12, 13 and 14 show the calculated contributions to the cross section when neglecting the relativistic corrections in the one-body current operator, i.e. when adopting $C_1(q, Q^2) = C_3(q, Q^2) = 1$ and $C_2(q, Q^2) = 0$ in Eq. (21). When comparing these curves with the solid ones one can estimate the effect of the relativistic corrections in the one-body current. For the transverse responses

σ_T and σ_{TT} the Foldy-Wouthuysen prescription does not lead to any relativistic correction into lowest order. Whereas the spin-orbit term in the charge-density operator produces rather small corrections in the longitudinal response σ_L in the considered kinematics, the longitudinal-transverse response σ_{LT} for the “stretched” single-particle states $1p_{3/2}$ and $1s_{1/2}$ is doubled after including the relativistic corrections in the charge-density operator. A strong sensitivity of the LT response to relativistic corrections was earlier found for $d(e, e'p)$ [63,68,69].

C. Neutron knockout

To our knowledge, beyond the giant resonance region no $(e, e'n)$ measurements have been made. Nevertheless, neutron knockout investigations with moderate energy resolution could be done at MAMI, BATES or TJNAF. Results for neutron knockout in kinematic conditions that can be reached with electron beam energies below 1 GeV are shown in Figure 17. These results are obtained with a neutron formfactor $G_E^n=0$. The $(e, e'n)$ calculations were done in the same kinematical conditions for the $(e, e'p)$ curves of Figure 7. The reduced cross sections for neutron knockout are subject to larger two-body current corrections than corresponding proton results. As a matter of fact, the absolute magnitude of the two-body current contributions is comparable for proton and neutron knockout. The fact that $(G_M^p/G_M^n)^2 \approx 2$ and the absence of a substantial neutron charge, however, makes them to be relatively more important in the neutron knockout channel. As could be expected on the basis of the isospin structure of the underlying current operators, the qualitative behaviour is similar for proton and neutron knockout. The net reduction of the cross sections displayed in Figure 17 is of the order 10-20%. Note that coupled-channel-effects between the proton knockout channels and the considerably weaker $(e, e'n)$ channels are expected to compensate largely for the loss of strength brought about by the meson and isobar degrees-of-freedom [10,70]. Our $(e, e'n)$ results are qualitatively similar to those reported in [14]. The MEC are observed to increase the cross section, an effect that is largely overcompensated by the isobaric current that works in the opposite direction. This reduction can be attributed to the fact that the one-body magnetization current and the isobaric current interfere destructively.

D. $^{208}\text{Pb}(e, e'p)$ results at $Q^2=0.3 \text{ (GeV/c)}^2$ and $x \approx 1$

In this section we report on calculations for an $^{208}\text{Pb}(e, e'p)$ experiment that was done at NIKHEF. This experiment was performed in very transverse kinematics ($\theta_e = 96^\circ$) at an incident electron energy of 462.14 MeV and near quasi-elastic conditions ($T_p=161 \text{ MeV}$, $x=0.94$). As this corresponds with very “transverse” kinematics we consider this as a worst-case-scenario benchmark for investigating the sensitivity to two-currents that could be expected in quasi-elastic $(e, e'p)$ from heavy nuclei. This is particularly important in view of the fact that the ^{208}Pb target is sometimes advocated as an appropriate surrogate for nuclear matter studies. In comparison with studies on light nuclei, for heavy nuclei there is a price to pay in that Coulomb distortion effects and reduced nucleon transparencies make both the electromagnetic and the FSI part of the reaction process more difficult to handle and subject to likely enhanced theoretical uncertainties. Here, we only want to study the *relative contribution* from the two-body currents that could be expected for a heavy nucleus like ^{208}Pb . For computational reasons we have neglected the Coulomb distortion effects. Indeed, an exact treatment of these would imply that the two-body matrix elements of Eq. (35) that involve a sum over all nucleons in the target nucleus, are to be calculated for a whole range of q values. Whereas calculations of this type could be performed at lower momentum transfer [17], the amount of multipoles required at higher momentum transfer makes it an enormous computational task. Figure 18 displays the reduced $^{208}\text{Pb}(e, e'p)$ cross section for knockout from the $3s_{1/2}$ and $2d_{5/2}$ orbits. It becomes clear that the predicted two-nucleon effects are modest and of the same relative size in comparison with the findings for light nuclei. Whereas the transparency for nucleon knockout has been established to decrease as the mass number increases [21] the impact of the two-body currents on single-nucleon knockout appears to be rather mass independent.

IV. SUMMARY AND CONCLUSIONS

Within the context of ongoing research activities in two-nucleon and pion production from nuclei a fair understanding of the two-nucleon currents in finite nuclei has been reached. With this knowledge the contribution of two-body currents to exclusive $(e, e'p)$ and $(e, e'n)$ reactions can be calculated with some confidence. Reasonable estimates of their contribution is essential in view of the fact that subnuclear d.o.f. frequently represent unwanted background that could be at the origin of ambiguities in the interpretation of $(\vec{e}, e'\vec{p})$ studies. Most of our investigations were carried out in quasi-elastic kinematics and momentum transfers $|\vec{q}| \leq 1 \text{ GeV/c}$. The effect of two-body currents dramatically

increases as one moves out of quasi-elastic conditions and/or higher missing momenta are probed. In quasi-elastic kinematics and the whole range of Q^2 values studied here, the two-body currents decrease the $(e, e'p)$ differential cross sections when lower missing momenta are probed. As the shape does not seem to be substantially affected by the two-body currents it appears virtually impossible to acquire experimental evidence for the role of two-body current effects from plain $(e, e'p)$ cross-section measurements in quasi-elastic kinematics. At the same time, our findings imply that the spectroscopic factors as they are usually derived from IA calculations are subject to corrections that would make them bigger. These corrections are not unimportant and exhibit a Q^2 dependence. Even at four-momentum transfers of $Q^2 \approx 0.8$ (GeV/c)² the effect of the two-body currents on the spectroscopic factor can be as large as 20%. The role of the two-body currents can be made more explicit by measuring the interference response functions that, admittedly, represent a rather small part in the total angular cross section. The induced polarization P_n exhibits a moderate sensitivity to the two-body currents at low missing momenta $p_m \leq 200$ MeV/c. Therefore, it retains its status as a proper variable to constrain the final-state interaction effects. Similar sort of sensitivities are found for the polarization transfer variables. In the light of exploiting these variables to increase our understanding of the (possible) medium dependency in the nucleon form factors, the effect of the meson and isobar degrees of freedom on the ratio $\frac{P'_t}{P_t}$ can be boiled down to a few percent at higher values of Q^2 . Under typical MAMI kinematics, which implies four-momentum transfers of the order $Q^2 \leq 0.50$ (GeV/c)², the impact of subnuclear degrees of freedom on the $\frac{P'_t}{P_t}$ ratio is predicted to be of the order of 10%. Of all pion-related two-body currents studied here the Δ -isobar current has by far the strongest impact on the $(\vec{e}, e'\vec{p})$ and $(e, e'n)$ observables. Multi-coincidence experiments of the type $(\gamma^{(*)}, NN)$ and $(\gamma^{(*)}, N\pi)$ at higher four-momentum transfers Q^2 would greatly help in further constraining the model assumptions with respect to the Δ -isobar current operator when reaching higher energy and momentum transfers.

Acknowledgement

This work was supported by the Fund for Scientific Research of Flanders under Contract No 4.0061.99 and the University Research Council.

-
- [1] J.J. Kelly, *Adv. Nucl. Phys.* **23** (1996) 75.
 - [2] V. Phandaripande, I. Sick and P.K.A. de Witt Huberts, *Rev. Mod. Phys.* **69** (1997) 981.
 - [3] D.H. Lu *et al.*, *Nucl. Phys.* **A634** (1998) 443.
 - [4] D.H. Lu *et al.*, *Phys. Lett.* **B417** (1998) 217.
 - [5] J.M. Laget, *Nucl. Phys.* **A579** (1994) 333.
 - [6] TJNAF experiment E89-003 "Measurement of Recoil Polarization in the ¹⁶O($e, e'p$) Reaction with 2.4 GeV Electrons" (spokesperson C. Glashauser).
 - [7] TJNAF experiment E93-043 "Polarization Transfer in the Reaction ⁴He($e, e'p$)³H in the Quasi-elastic Scattering Region" (spokesperson J. Van Den Brand)
 - [8] TJNAF experiment E91-006 "Study of Nuclear Medium Effects by Recoil Polarization up to High Momentum Transfers" (spokesperson A. Saha)
 - [9] J.J. Kelly, *Phys. Rev. C* **56** (1997) 2672.
 - [10] J.J. Kelly, nucl-th/980990
 - [11] Toshio Suzuki, *Nucl. Phys.* **A495** (1989) 581.
 - [12] S. Boffi, C. Giusti, F.D. Pacati and M. Radici, *Nucl. Phys.* **A518** (1990) 639.
 - [13] S. Boffi and M. Radici, *Phys. Lett.* **B242** (1990) 151.
 - [14] S. Boffi, M. Radici, J.J. Kelly and T.M. Payerle, *Nucl. Phys.* **A539** (1992) 597.
 - [15] M.B. Epstein *et al.*, *Phys. Rev. Lett.* **70** (1993) 2868.
 - [16] V. Van der Sluys, J. Ryckebusch and M. Waroquier, *Phys. Rev. C* **54** (1996) 1322.
 - [17] V. Van der Sluys, J. Ryckebusch and M. Waroquier, *Phys. Rev. C* **49** (1994) 2695.
 - [18] A.S. Raskin and T.W. Donnelly, *Ann. of Phys.* **191** (1989) 78.
 - [19] A. Picklesimer and J.W. Van Orden, *Phys. Rev. C* **35** (1987) 266.
 - [20] S. Boffi, C. Giusti, F.D. Pacati and M. Radici, *Electromagnetic Response of Atomic Nuclei*, Oxford Studies in Nuclear Physics (Clarendon Press, Oxford, 1996).
 - [21] D. Potterfeld *et al.*, in *Proceedings of the Conference on Perspectives in Hadronic Physics*, edited by S. Boffi, C. Ciofi degli Atti and M. Giannini, (World Scientific, Singapore, 1998), 164.
 - [22] J. Ryckebusch, M. Waroquier, K. Heyde, J. Moreau and D. Ryckbosch, *Nucl. Phys.* **A476** (1988) 237.
 - [23] C. Mahaux and H. Weidenmüller, *in Shell model approach to nuclear reactions* (North-Holland, Amsterdam, 1969).

- [24] J.E. Amaro, M.B. Barbaro, J.A. Caballero, T.W. Donnelly and M. Molinari, Nucl. Phys. **A643** (1998) 349.
- [25] H.W. Fearing, G.I. Poulis and S. Scherer, Nucl. Phys. **A570** (1994) 657.
- [26] S. Boffi, F. Capuzzi, P. Demetriou and M. Radici, Nucl. Phys. **A637** (1998) 585.
- [27] S. Jeschonnek and T.W. Donnelly, Phys. Rev. C **57** (1998) 2483.
- [28] Yanhe Jin and D.S. Onley, Phys. Rev. C **50** (1994) 377.
- [29] J.M. Udiás, P. Sarriguren, E. Moya de Guerra, E. Garrido and J.A. Caballero, Phys. Rev. C **48** (1993) 2731.
- [30] M. Hedayati-Poor, J.I. Johansson and H.S. Sheriff, Phys. Rev. C **51** (1995) 2044.
- [31] J.P. McDermott, Phys. Rev. Lett. **65** (1990) 1991.
- [32] J. Carlson and R. Schiavilla, Rev. Mod. Phys. **70** (1998) 743.
- [33] J. Ryckebusch, V. Van der Sluys, K. Heyde, H. Holvoet, W. Van Nespén, M. Waroquier and M. Vanderhaeghen, Nucl. Phys. **A624** (1997) 581.
- [34] L.E. Marcucci, D.O. Riska and R. Schiavilla, Phys. Rev. C **58** (1998) 3069.
- [35] P. Stoler, Phys. Rep. **226** (1993) 103.
- [36] V.V. Frolov *et al.*, Phys. Rev. Lett. **82** (1999) 45.
- [37] E. Oset, H. Toki and W. Weise, Phys. Rep. **83** (1982) 281.
- [38] M.J. Dekker, P.J. Brussaard and J.A. Tjon, Phys. Rev. C **49** (1994) 2650.
- [39] T. Wilbois, P. Wilhelm, and H. Arenhövel, Phys. Rev. C **54** (1996) 3311.
- [40] J. Ryckebusch, L. Machenil, M. Vanderhaeghen, V. Van der Sluys, and M. Waroquier, Phys. Rev. C **54** (1996) 3313.
- [41] B. Körfgen, P. Oltmanns, F. Osterfeld and T. Udagawa, Phys. Rev. C **55** (1997) 1819. Rev. C **50** (1994) 1637.
- [42] N. Bianchi *et al.*, Phys. Rev. C **54** (1996) 1688.
- [43] J.K. Koch and N. Ohtsuka, Nucl. Phys. **A435** (1985) 765 and J. Koch *in* Moderns Topics in Electron Scattering, Eds. B. Frois and I. Sick, (World Scientific, Singapore) (1991) 28.
- [44] J.S. O'Connell *et al.*, Phys. Rev. C **35** (1987) 1063.
- [45] R. Cenni, P. Christillin and G. Dillon, Phys. Lett. **B139** (1984) 341.
- [46] B. Körfgen, F. Osterfeld and T. Udagawa, Phys. Rev. C **50** (1994) 1637.
- [47] C.R. Chen and T.-S.H. Lee, Phys. Rev. C **38** (1988) 2187.
- [48] L.A. Kondratyuk, M.I. Krivoruchenko, N. Bianchi, E. De Sanctis and V. Muccifora, Nucl. Phys. **A579** (1994) 453.
- [49] E. Oset and L.L. Salcedo, Nucl. Phys. **A468** (1987) 631.
- [50] I.J.D. MacGregor *et al.*, Phys. Rev. Lett. **80** (1998) 245.
- [51] J. Ryckebusch, M. Vanderhaeghen, L. Machenil and M. Waroquier, Nucl. Phys. **A568** (1994) 828-854.
- [52] G. Rosner, *in* Proc. Conf. on Perspectives in Hadronic Physics, ICTP Trieste, Italy, May 12-16, 1997, eds. S. Boffi, C. Ciofi degli Atti and M.M. Gianninni (World Scientific, Singapore) 185. P. Bartsch *et al.*, "Investigation of short-range nucleon-nucleon correlations using the reaction $^{16}O(e,e'pp)^{14}C$ in super-parallel kinematics" MAMI proposal A1/1-97 (spokesperson G. Rosner), 1997.
- [53] G. Kaschl, G. Mairle, H. Mackh, D. Hartwig and U. Schwinn, Nucl. Phys. **A178** (1971) 275.
- [54] C.J.G. Onderwater *et al.*, Phys. Rev. Lett. **81** (1998) 2213.
- [55] C.C.Gearhart, PhD thesis, Washington University (St. Louis, 1994), unpublished and W. Dickhoff, private communication.
- [56] K.I. Blomqvist *et al.*, Phys. Lett. **B421** (1998) 71.
- [57] K.I. Blomqvist *et al.*, Phys. Lett. **B344** (1995) 85.
- [58] T. de Forest, Nucl. Phys. **A392** (1983) 232.
- [59] L.J.H.M. Kester *et al.*, Phys. Lett. **B366** (1996) 44.
- [60] G. Garino *et al.*, Phys. Rev. C **45** (1992) 780.
- [61] M. Leuschner *et al.*, Phys. Rev. C **49** (1994) 955.
- [62] J.A. Caballero, T.W. Donnelly, E. Moya de Guerra and J.M. Udiás, Nucl. Phys. **A643** (1998) 189.
- [63] S. Gilad, W. Bertozzi and Z.-L. Zhou, Nucl. Phys. **A631** (1998) 276c.
- [64] J. Mandeville *et al.*, Phys. Rev. Lett. **72** (1994) 3325.
- [65] R.J. Woo *et al.*, Phys. Rev. Lett. **80** (1998) 456.
- [66] B.D. Milbrath *et al.*, Phys. Rev. Lett. **80** (1998) 452.
- [67] J.J. Kelly, Adv. Nucl. Phys. **23** (1996) 75.
- [68] E. Hummel and J.A. Tjon, Phys. Rev. C **49** (1994) 21.
- [69] J.E. Ducret *et al.*, Phys. Rev. C **49** (1994) 1783.
- [70] J. Ryckebusch, K. Heyde, D. Van Neck and M. Waroquier, Nucl. Phys. **A503** (1989) 694.

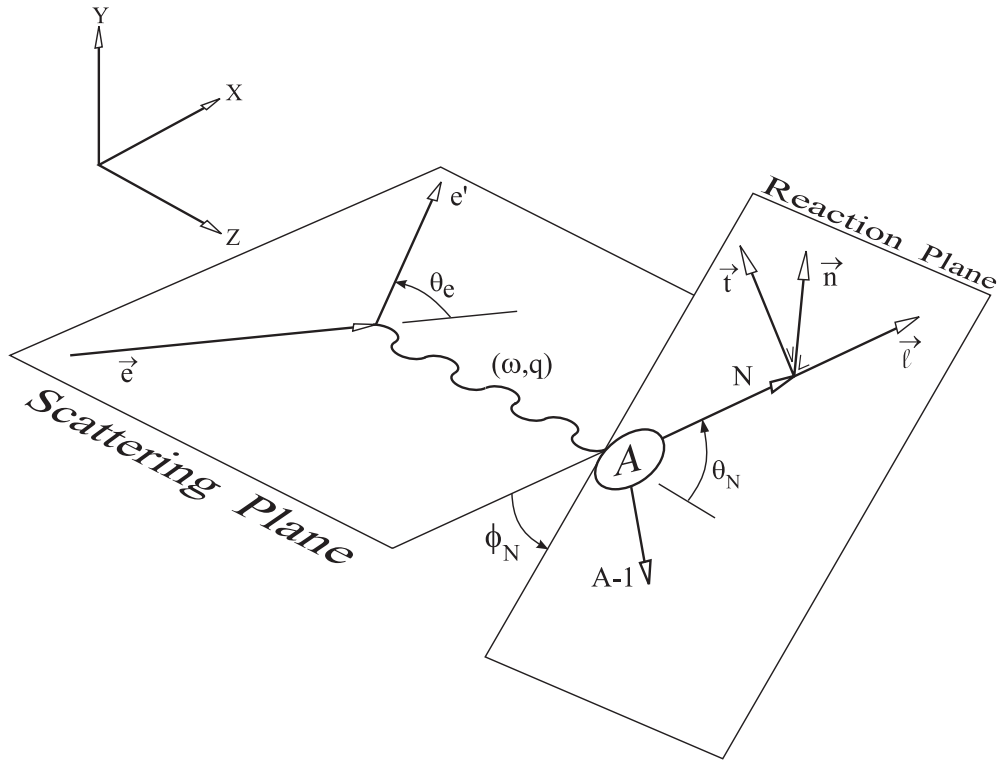


FIG. 1. Diagram of the $(e, e'p)$ process showing the electron scattering plane, the reaction plane and the basis in which the ejectile's polarization is determined.

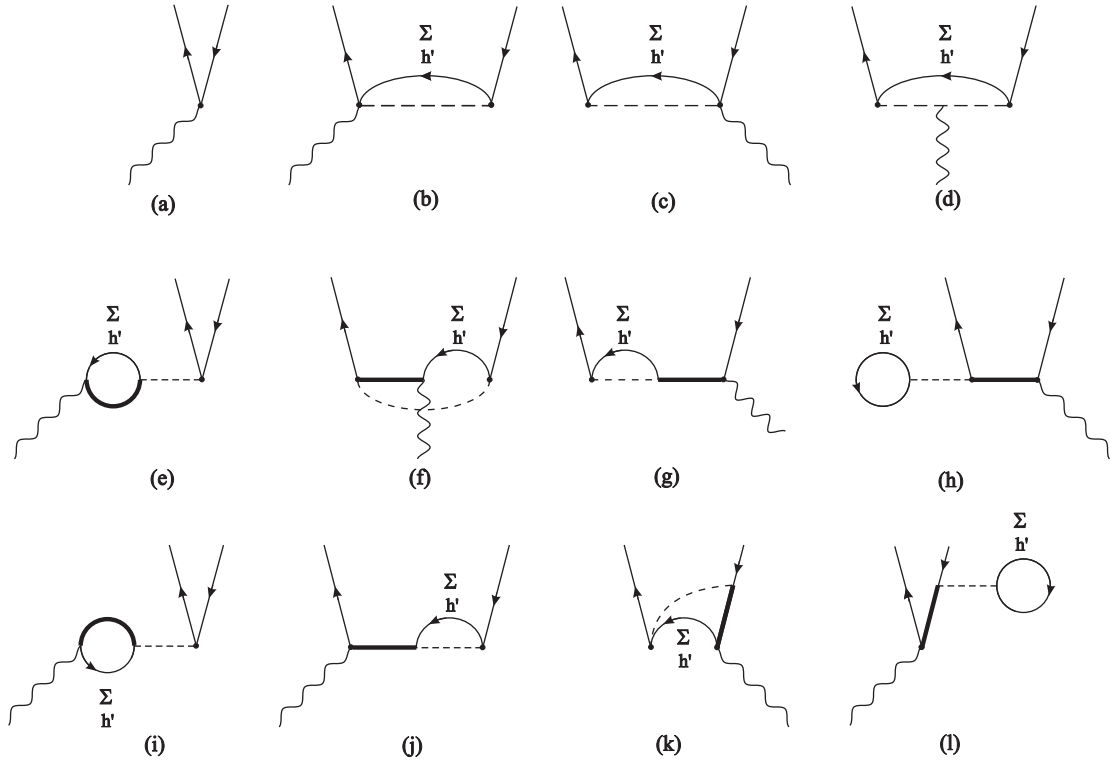


FIG. 2. Diagrammatic representation of the reaction processes included in the $A(\vec{e}, e'\vec{p})$ calculations. Wavy, thin, thick and dashed lines denote photons, nucleons, Δ 's and pions. Nucleon lines with an arrow down (up) refer to occupied (scattering) states. Diagram (a) refers to the conventional IA. Diagrams (b)-(d) are related to the MEC, whereas (e)-(l) represent the different direct and exchange IC contributions.

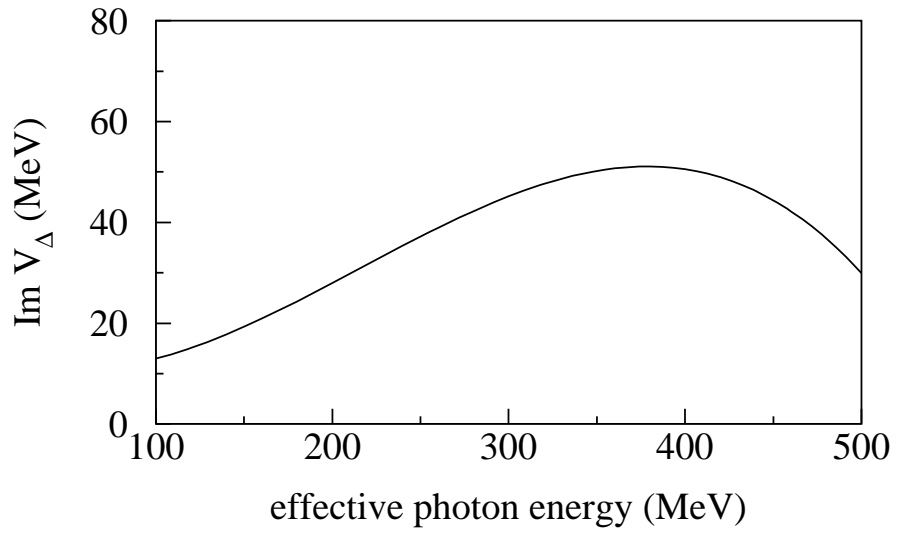


FIG. 3. The imaginary part of the Δ -medium potential as a function of the effective photon energy ($=\omega - \frac{q^\mu q_\mu}{2M_N}$) for full nuclear density. The parametrization is from Reference [49].

$^{16}\text{O}(e,e'pp)^{14}\text{C}$; $\omega=210$ MeV ; $q=300$ MeV/c

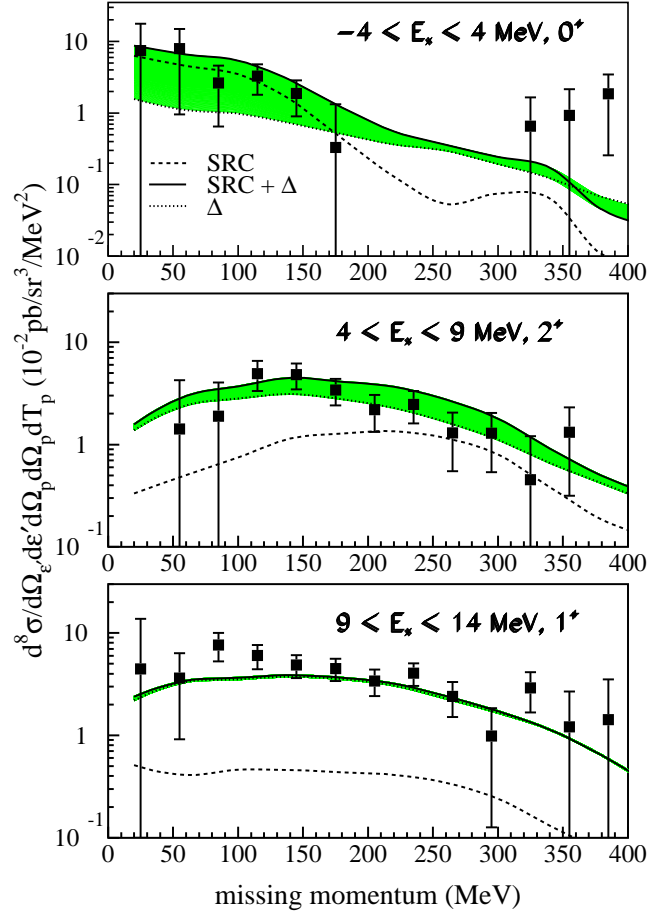


FIG. 4. Calculated $^{16}\text{O}(e,e'pp)$ missing momentum distributions for various groups of final states and electron kinematics determined by $\epsilon=580$ MeV, $\epsilon'=374$ MeV and $\theta_e=26.2^\circ$. The data and curves refer to the two-proton knockout phase-space determined by the polar angles $8^\circ \leq \theta_1 \leq 40^\circ$, $115^\circ \leq \theta_2 \leq 155^\circ$ and the kinetic energy of the backward going proton $52 \text{ MeV} \leq T_2 \leq 108 \text{ MeV}$. The polar angles are expressed relative to the direction of the momentum transfer. For the calculations, five mesh points were considered in each of these variables and phase-space averaging was pursued. The data are from Ref. [54]. The solid line is the result of the distorted-wave calculation when both the SRC and Δ isobar effects are included. The dotted (dashed) line includes solely the Δ isobar (SRC) effects.

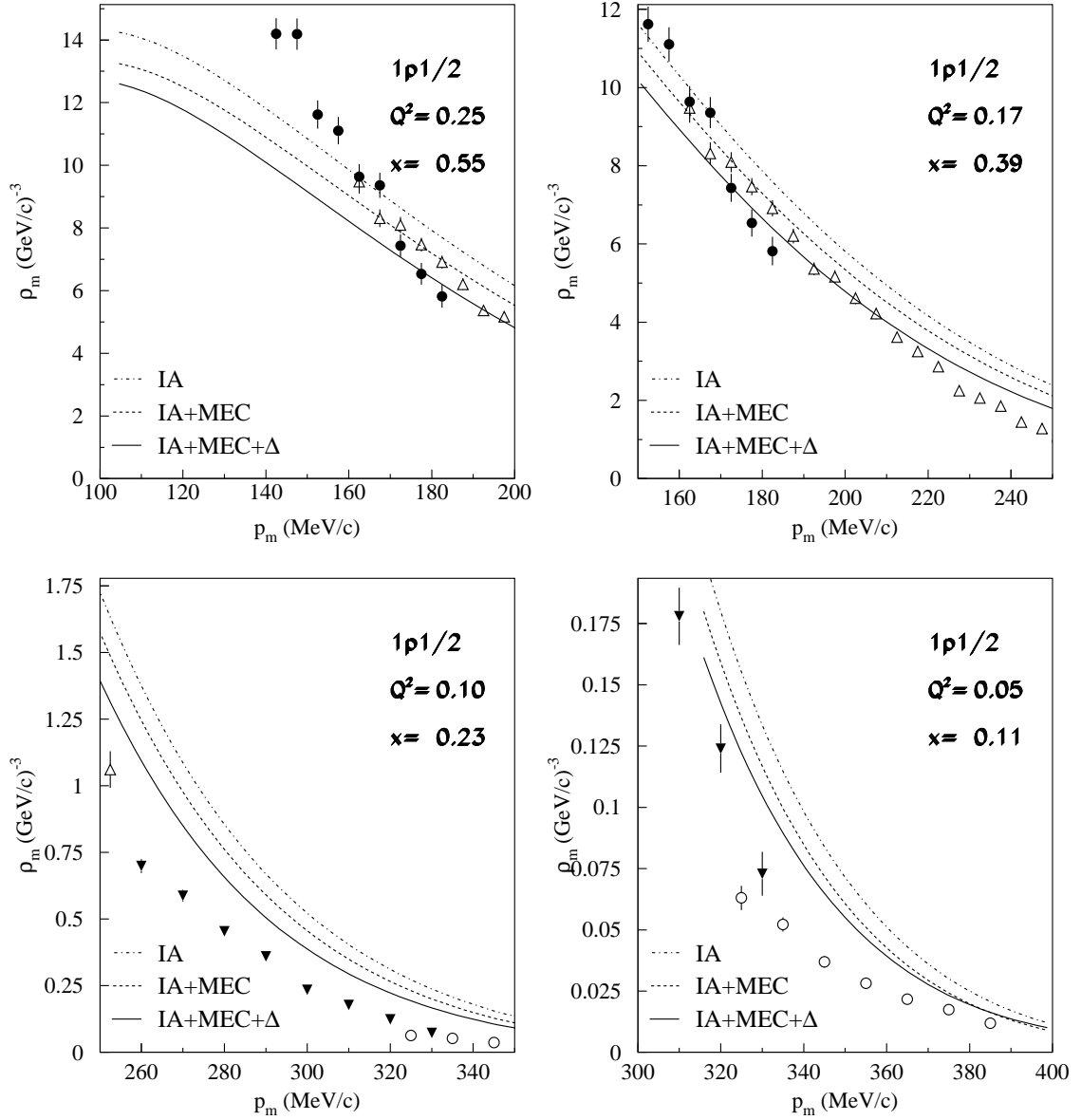


FIG. 5. Reduced cross sections for the $^{16}\text{O}(e, e'p)^{15}\text{N}(1/2^-, \text{g.s.})$ reaction in parallel kinematics. The initial electron energy is kept constant at $\epsilon=855.1$ MeV. Starting from the upper left panel and going clockwise the momentum transfer q is respectively 0.55, 0.47, 0.39 and 0.3 GeV/c. The dot-dashed curve shows the result for the impulse approximation ; in the dashed curve MEC effects are also included, and the solid curve represents the full calculation including also IC. For each case a central value of Q^2 and Bjorken x is given.

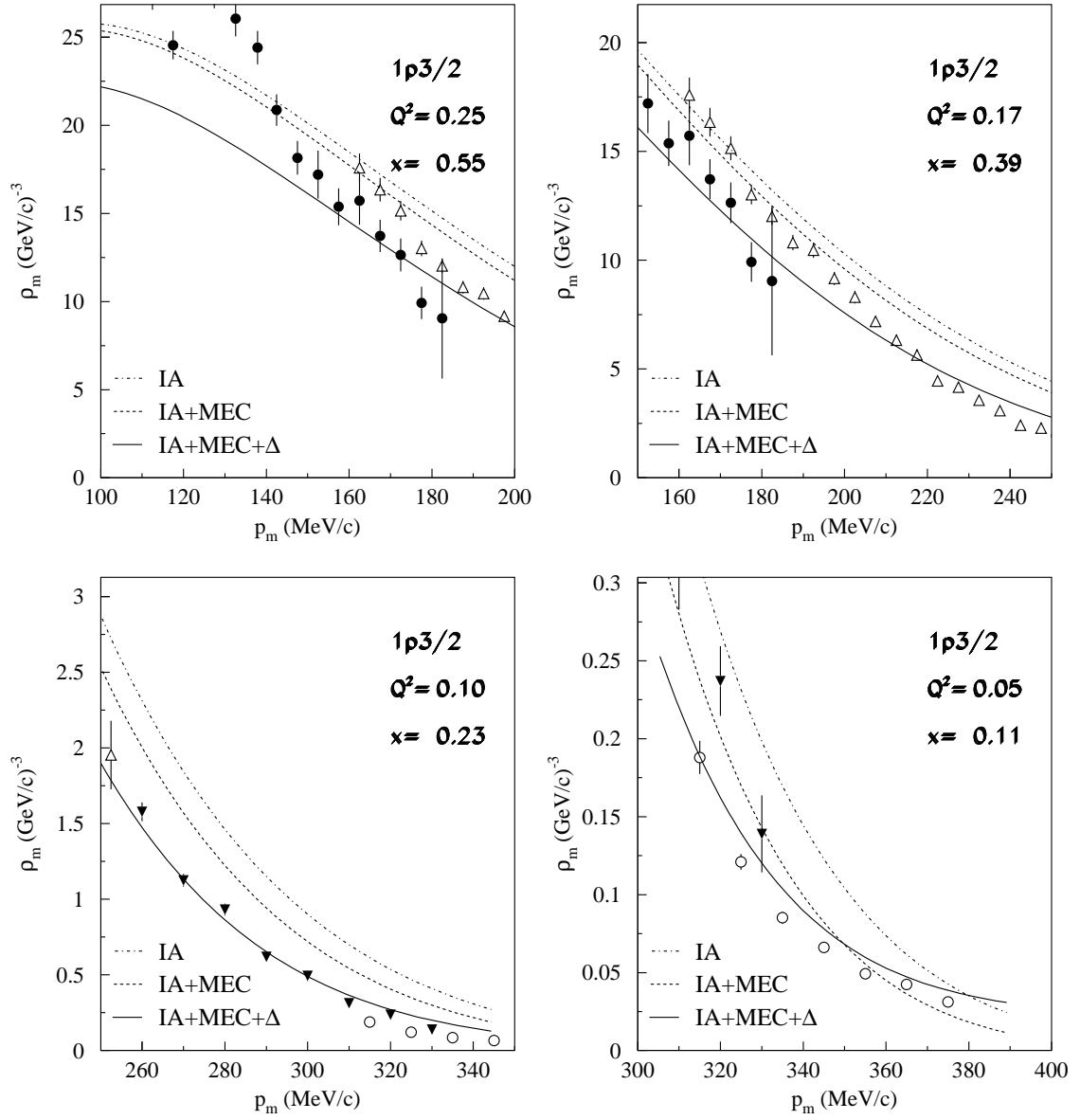


FIG. 6. As in Figure 5, but now for the $^{16}\text{O}(e, e'p)^{15}\text{N}(3/2^-, 6.32 \text{ MeV})$ transition.

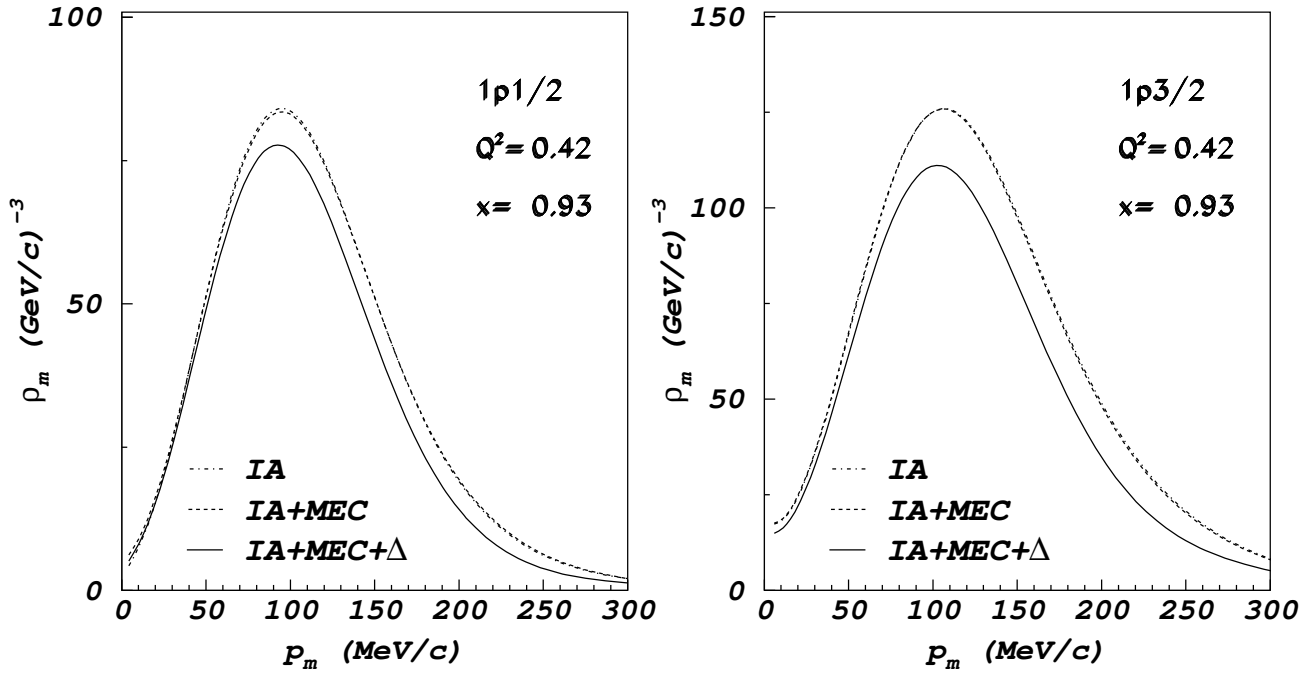


FIG. 7. Reduced cross sections for $^{16}\text{O}(e, e'p)$ from p-shell states in quasi-perpendicular kinematics. The electron kinematics is determined by $\epsilon=0.855$ GeV, $\omega=240$ MeV and $q=0.69$ GeV/c. The dot-dashed curve shows the result for the impulse approximation ; in the dashed curve MEC effects are also included, and the solid curve represents the full calculation including also IC. The curves are normalized for full p-shell occupancy.

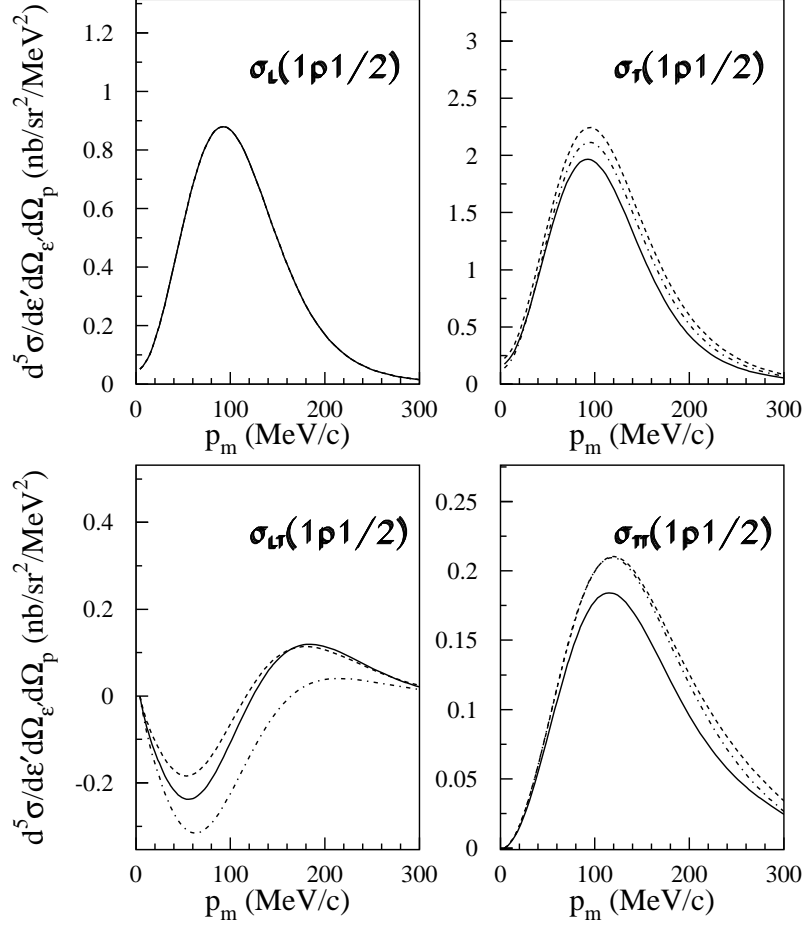


FIG. 8. The different contributions to the $^{16}\text{O}(e, e'p)^{15}\text{N}(1/2^-)$ cross section for the kinematics of Figure 7. The dot-dashed curve shows the result for the impulse approximation ; in the dashed curve MEC effects are also included, and the solid curve represents the full calculation including also IC. The curves are normalized for full $1p_{1/2}$ occupancy.

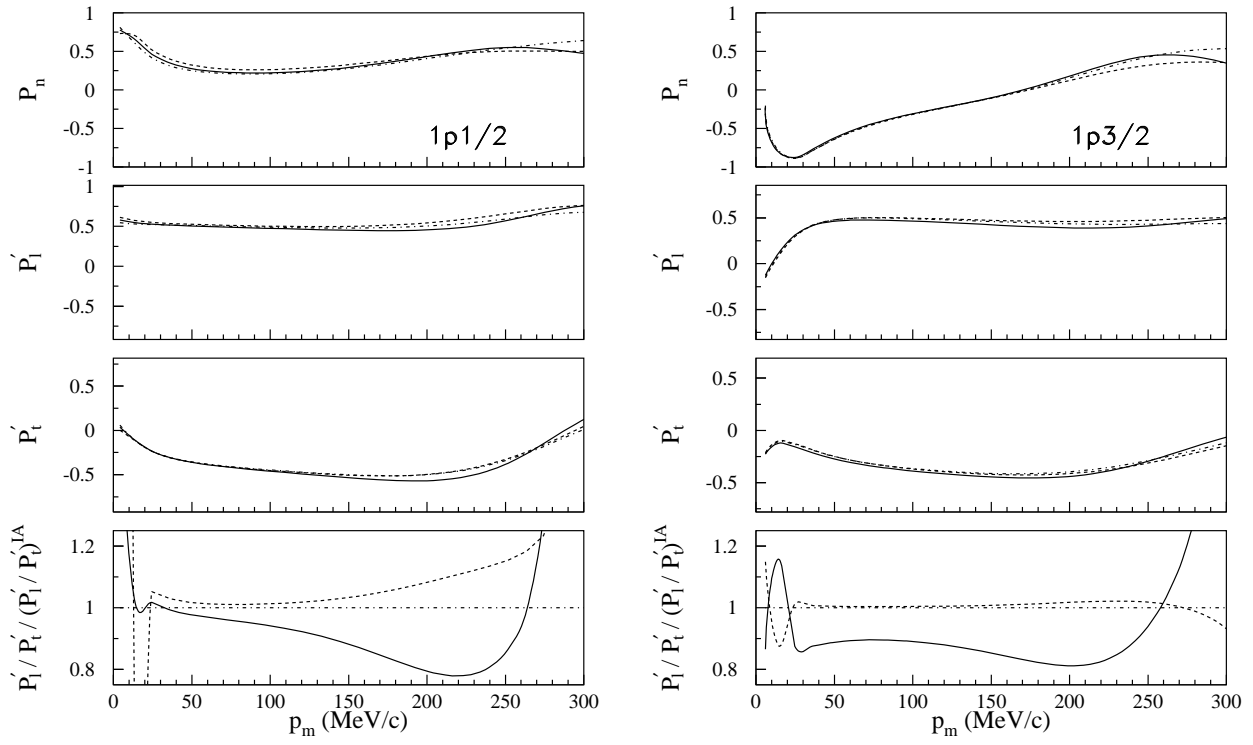


FIG. 9. The recoil polarization observables for the kinematics of Figure 7. Same line conventions as in Figure 8.

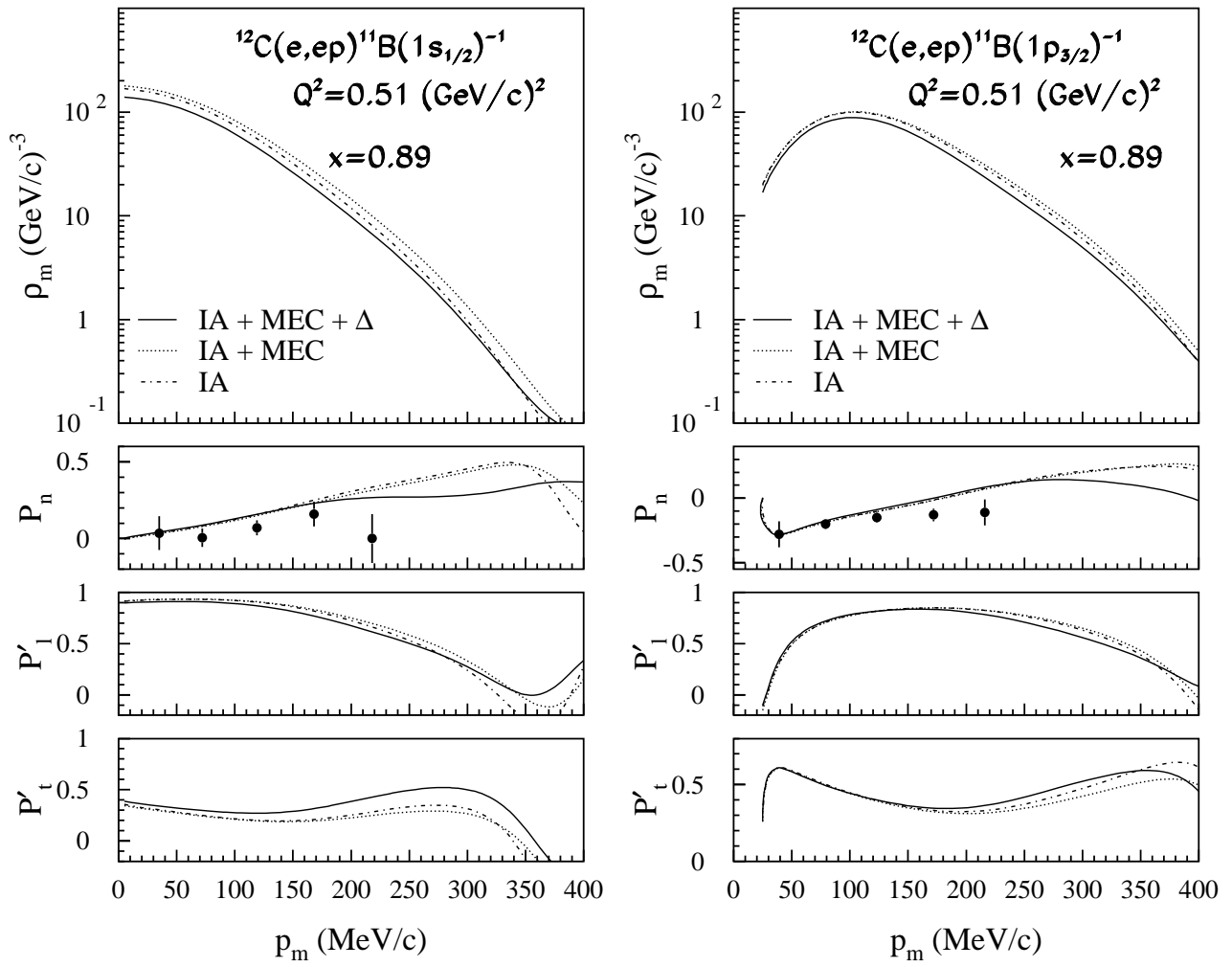


FIG. 10. Reduced cross section and recoil polarization observables for $^{12}\text{C}(e, e'p)$ in quasi-perpendicular kinematics. The initial electron energy is $\epsilon=579$ MeV, $\omega=290$ MeV and $q=0.76$ GeV/c. The reduced cross sections are normalized for full $1p_{3/2}$ and $1s_{1/2}$ occupancy. The data are from Ref. [65].

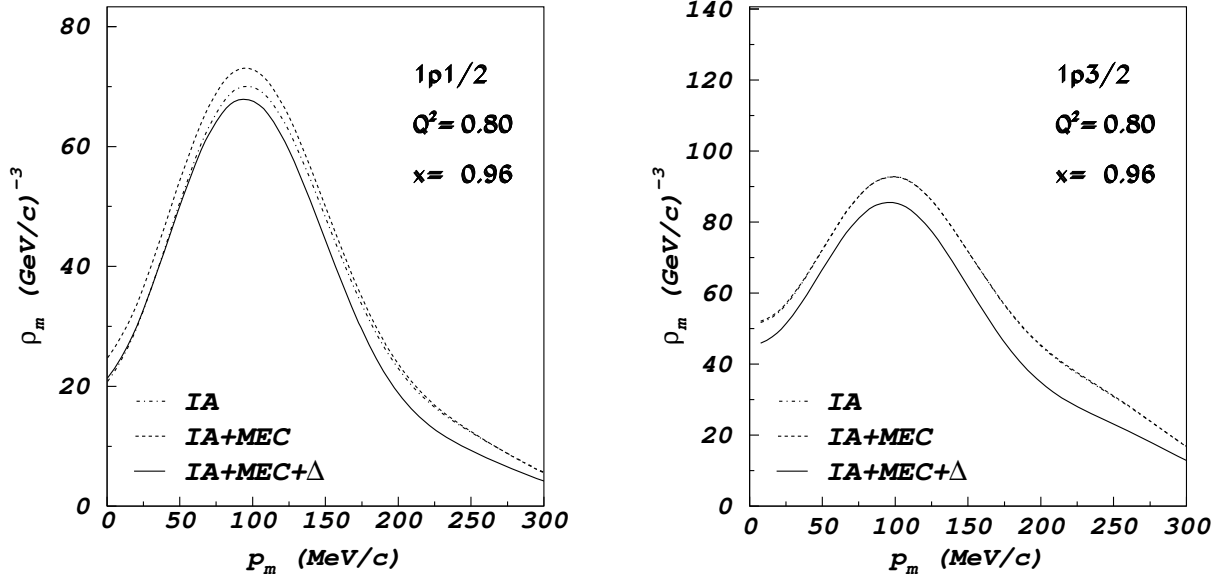


FIG. 11. Reduced cross sections for $^{16}\text{O}(e, e'p)$ from p-shell states in quasi-perpendicular kinematics. The electron kinematics is determined by $\epsilon=2.445$ GeV, $\omega=445$ MeV and $q=1$ GeV/c. The dot-dashed curve shows the result for the impulse approximation ; in the dashed curve MEC effects are also included, and the solid curve represents the full calculation including also IC.

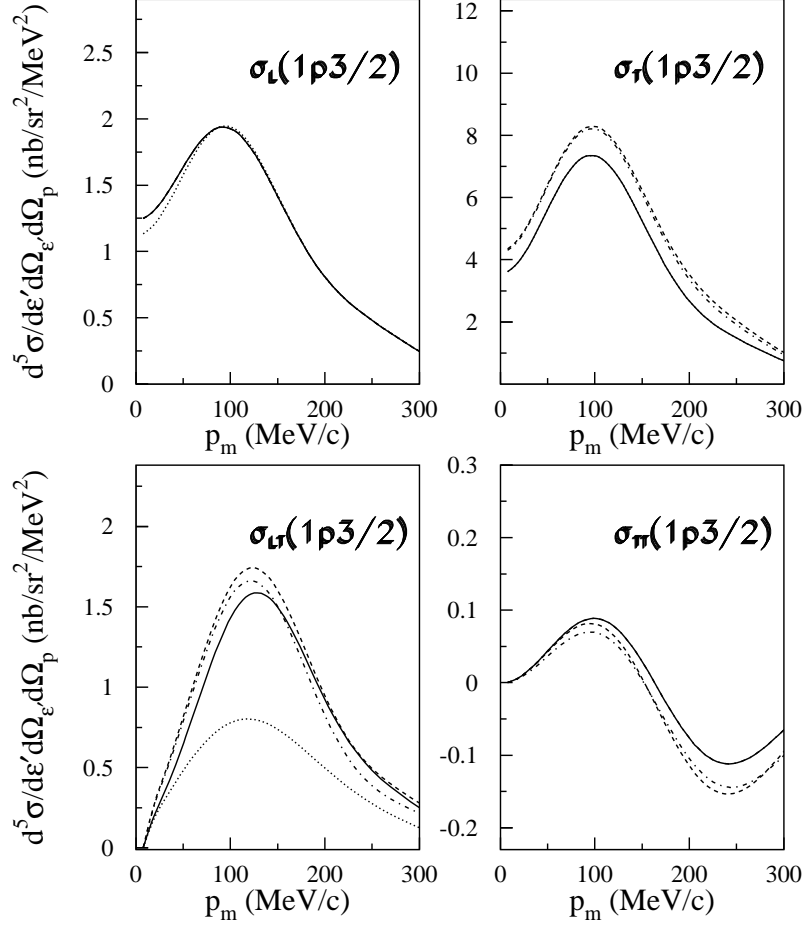


FIG. 12. The various structure functions in $^{16}\text{O}(e, e'p)$ for $1p_{3/2}$ knockout in quasi-perpendicular kinematics. The electron kinematics is determined by $\epsilon=2.445$ GeV, $\omega=445$ MeV and $q=1$ GeV/c. The dot-dashed curve shows the result for the impulse approximation ; in the dashed curve MEC effects are also included, and the solid curve represents the full calculation including also IC. The dotted line is the result of the full calculation when neglecting the relativistic corrections in the current operator.

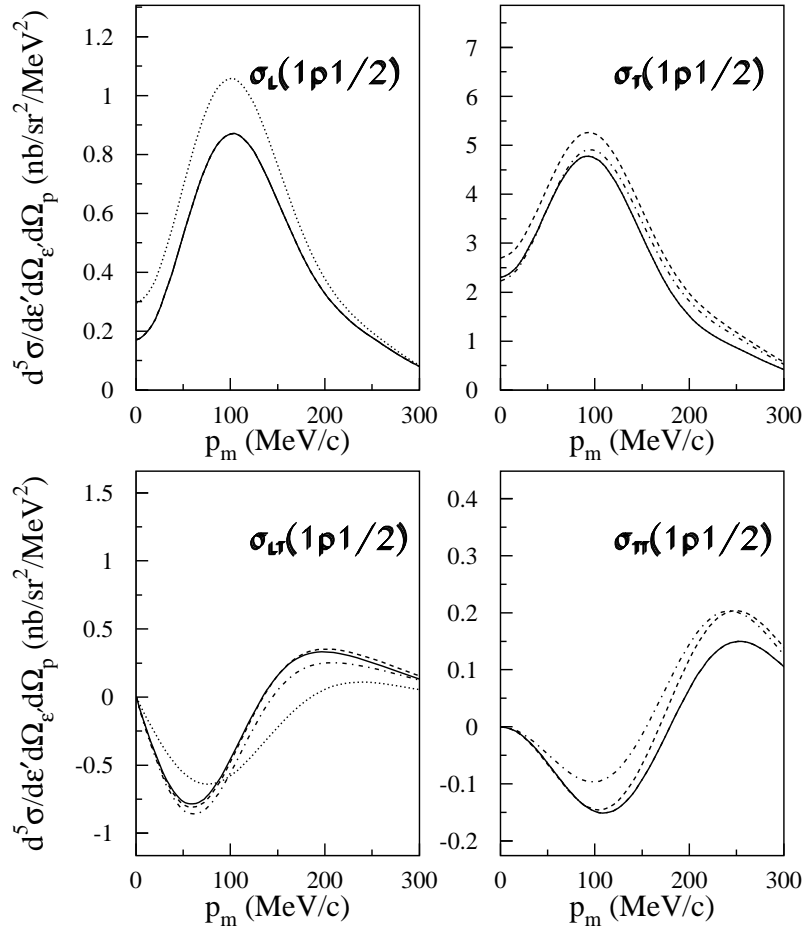


FIG. 13. As in Figure 12 but now for knockout from the $1p_{1/2}$ orbital.

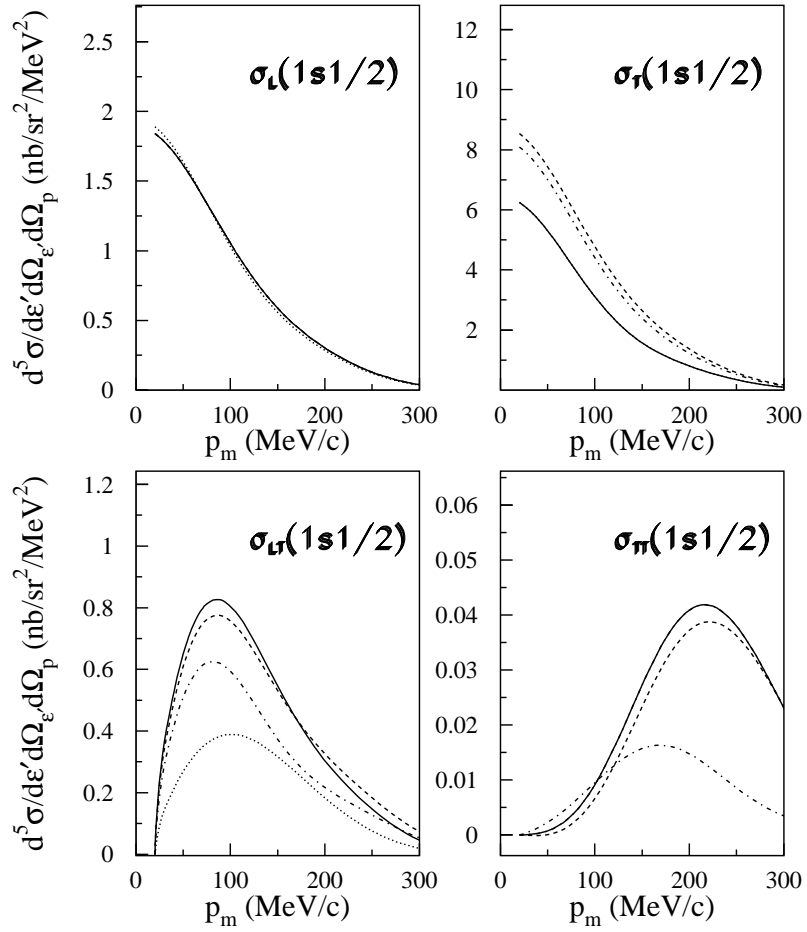


FIG. 14. As in Figure 12 but now for knockout from the $1s_{1/2}$ orbital.

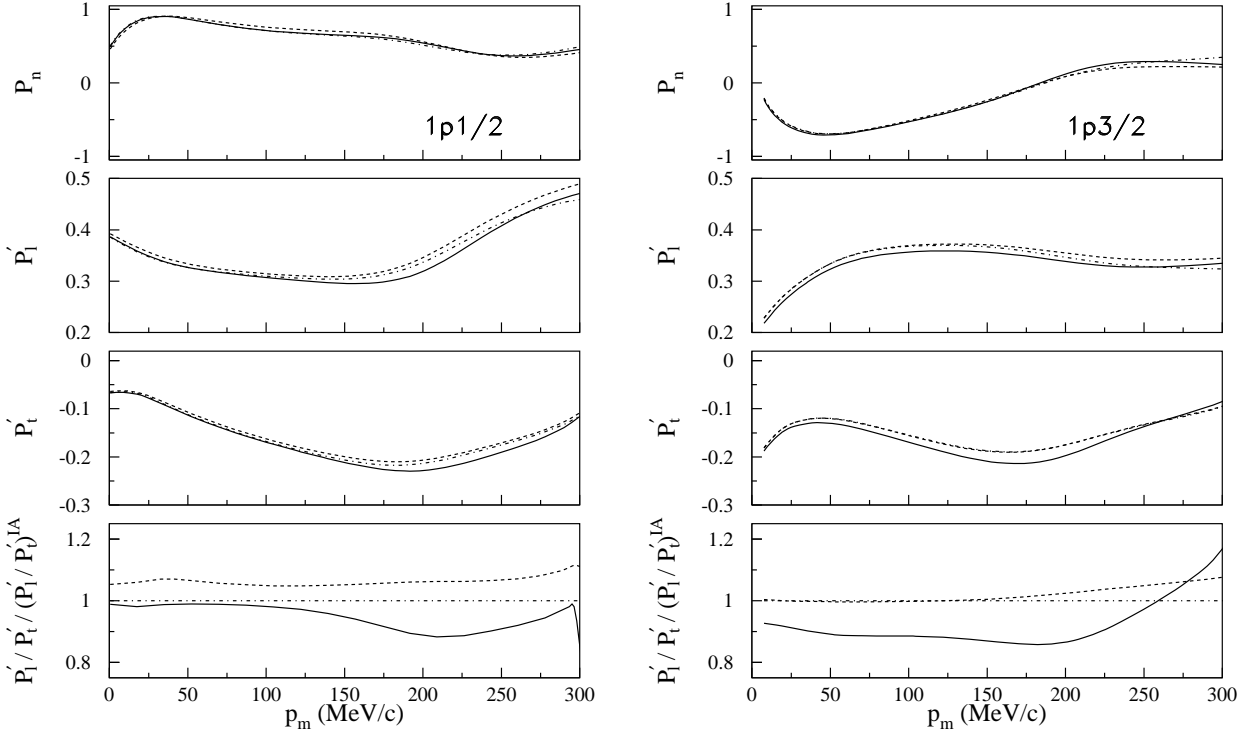


FIG. 15. Recoil polarization observables as a function of the missing momentum in quasi-perpendicular kinematics for knockout from the p-shell orbits in the $^{16}\text{O}(\bar{e}, e'\bar{p})$ reaction at $\epsilon=2.445$ GeV, $\omega=445$ MeV and $q=1$ GeV/c. The dot-dashed curve shows the result for the impulse approximation ; in the dashed curve MEC effects are also included, and the solid curve represents the full calculation including also IC.

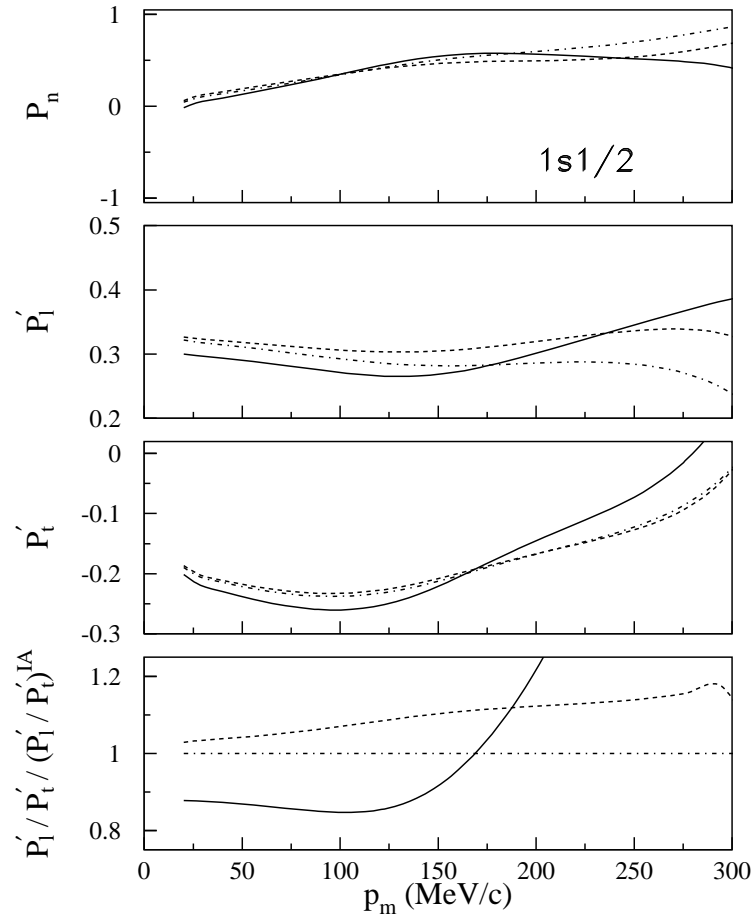


FIG. 16. As in Figure 15 but for knockout from the $1s_{1/2}$ orbit.

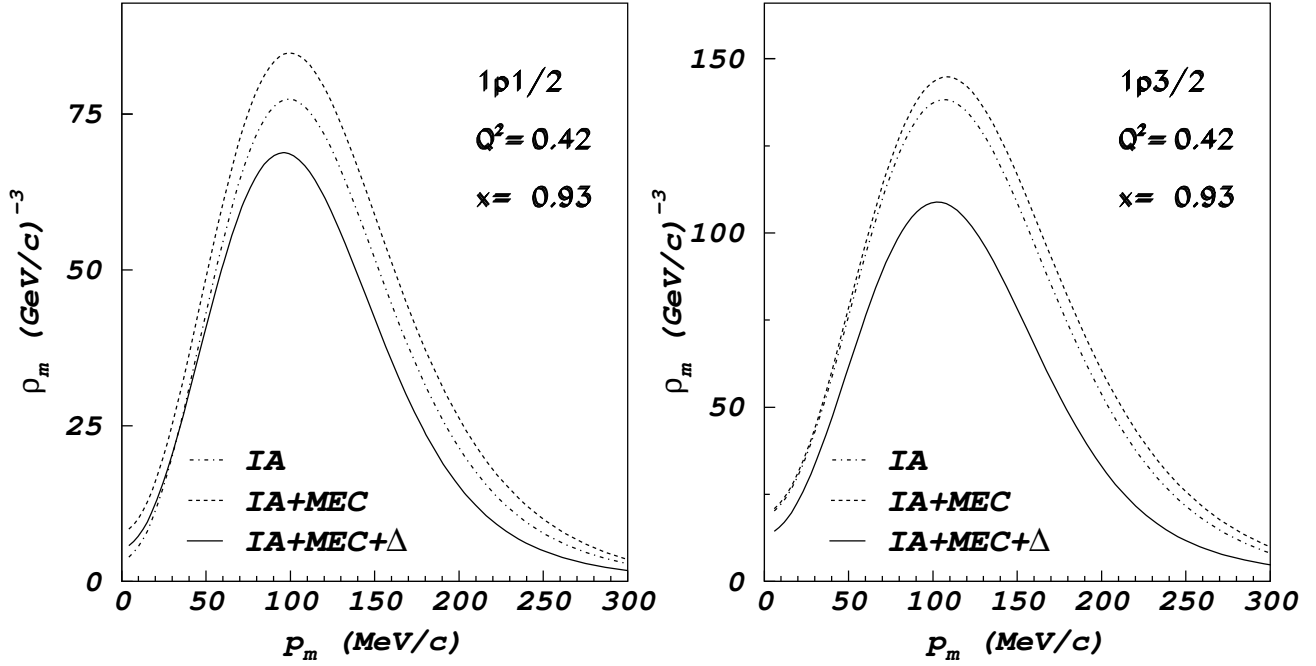


FIG. 17. Reduced cross sections for $^{16}\text{O}(e, e'n)$ from p-shell states in quasi-perpendicular kinematics. The electron kinematics is determined by $\epsilon=0.855$ GeV, $\omega=240$ MeV and $q=0.69$ GeV/c. The dot-dashed curve shows the result for the impulse approximation ; in the dashed curve MEC effects are also included, and the solid curve represents the full calculation including also IC. The curves are normalized for full sub-shell occupancy.

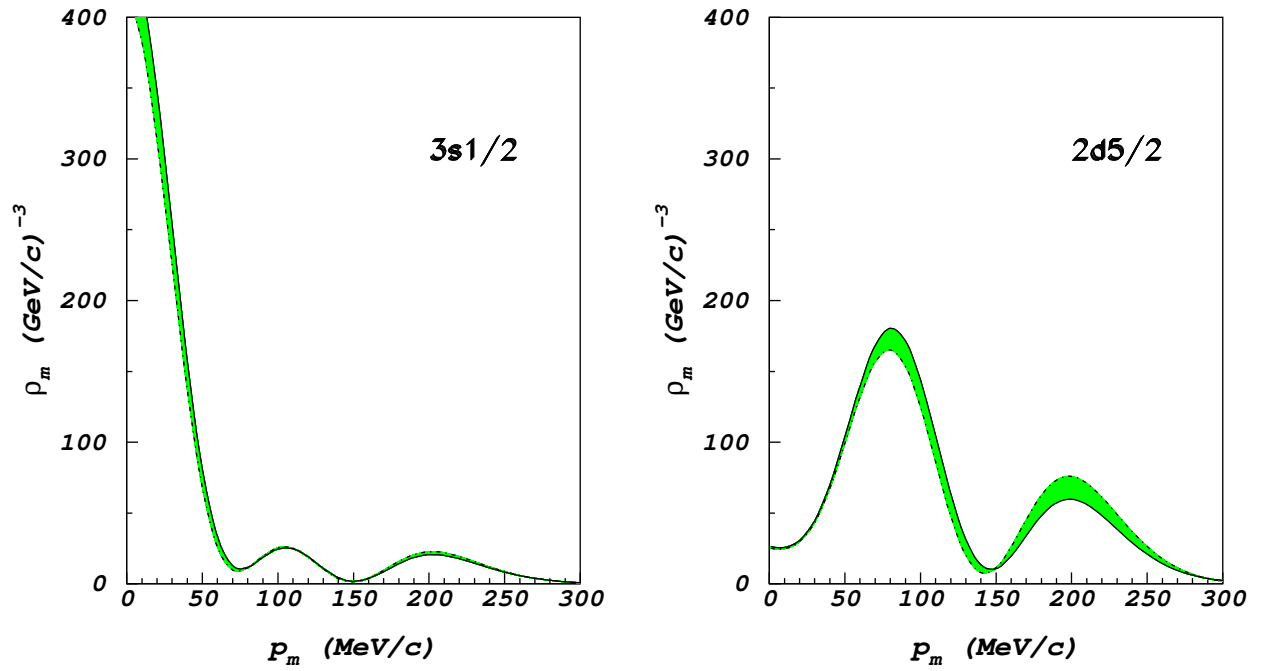


FIG. 18. Reduced cross sections for $^{208}\text{Pb}(e, e'p)$ from in quasi-perpendicular kinematics. The electron kinematics is determined by $\epsilon=0.462$ GeV, $\omega=170$ MeV and $q=0.57$ GeV/c. The dot-dashed curve shows the result for the impulse approximation, whereas the solid curve is the result of a calculation that includes also MEC and IC. The curves are normalized for full sub-shell occupancy.